



Modification of optoelectronic properties of conjugated oligomers due to donor/acceptor functionalization: DFT study

Andriy Zhugayevych ^{a,*}, Olena Postupna ^b, Hsing-Lin Wang ^b, Sergei Tretiak ^{b,a}

^a Skolkovo Institute of Science and Technology, Moscow 143026, Russia

^b Theoretical Division, Los Alamos National Laboratory, NM 87545, United States



ARTICLE INFO

Article history:

Available online 7 September 2016

Keywords:

Functionalized p-phenylene vinylene
Distyrylbenzene
Molecular descriptor
Push–pull functionalization
Structure–property relationship

ABSTRACT

A comprehensive DFT study of a set of oligo(p-phenylene vinylene) molecules is performed to understand the structural and electronic changes upon functionalization. These changes are rationalized within a model considering frontier molecular orbitals of the π -conjugated system and σ -bonding orbital by which the functional group is attached to the host molecule. Two simple scalar quantum chemical descriptors are shown to correlate with optoelectronic properties of the functionalized molecule: the electronegativity and the relative electric dipole moment of the smallest π -closed shell subsystem containing the functional group and the terminal segment of the host molecule (phenyl). Both descriptors correlate linearly with the empirical Hammett σ_p constant for a set of 24 functional groups. Comparison with available experimental data on UV-vis absorption and cyclic voltammetry is made. Observed structural changes reflect changes in the electronic density.

© 2016 Elsevier B.V. All rights reserved.

1. Introduction

Functionalization of conjugated molecules is routinely used for tailoring their properties for purposes of organic electronics [1] and other applications. Due to presence of an extended π -conjugated system, small local changes in molecular composition may lead to large changes in physical properties of the whole molecule. Recently [2,3] it was experimentally demonstrated that changes in the end group of an oligo(p-phenylene vinylene) molecule strongly influence optical properties of the oligomer. Although this phenomenon is not novel, and functionalized conjugated molecules, especially of phenylene vinylene family, have been extensively investigated both theoretically (see general references [4–7], optical spectra [8–10], nonlinear optical response [11,12], cations [13], functionalized oligomers [14–17]) and experimentally [18–22], the underlying mechanisms of how functionalization changes molecular properties have been rarely analyzed on the

basis of first-principle calculations [23,24]. The present paper aims to fill this gap for the case of linearly extended π -conjugated systems. In such systems universal relations between structural and electronic properties emerge upon separation of electronic π -system from the rest of the molecular orbitals (MO). In particular, we take advantage of the detailed experimental characterization of a set of p-phenylene vinylene oligomers [2] to perform in-depth first-principles investigation of this system to understand and rationalize the dependence of the molecular properties on the functional group. The molecular structure is shown in fig. 1. Here we refer to all the functionalized p-phenylene vinylene oligomers with the three phenyl rings as OPV3, or R-OPV3 if a specific functional group is discussed.

It should be clarified that qualitatively on a coarse grained level we understand how functional group influences electronic properties of the host molecule. The question addressed here is to quantify this influence and analyze multitude of tiny yet robust fingerprints in the host molecule. In particular, it is useful to have a single molecular descriptor correlating with the changes of electronic properties upon functionalization. The problem is that combinations of basic electronic descriptors such as ionization potential (IP) and electron affinity (EA) of a functional group, either as radical or hydrogen-passivated, do not correlate with electronic properties of the functionalized OPV3 (see Supporting Information, Fig. S1). At the other hand, good statistical correlation can always

Abbreviations: BLA, bond length alternation; DFT, density functional theory; EA, electron affinity; HOMO, highest occupied MO; IP, ionization potential; LUMO, lowest occupied MO; LR, linear response; MO, molecular orbital; NO, natural orbital; NTO, natural transition orbital; OPV3, oligo(p-phenylene vinylene) with 3 phenyl rings; PES, potential energy surface; SS, state specific; TDDFT, time dependent DFT.

* Corresponding author.

E-mail address: a.zhugayevych@skoltech.ru (A. Zhugayevych).

be achieved through cheminformatics using large enough set of empirical or quantum chemical descriptors [25]. Of them, the so called Hammett σ_p constant [25–27] is expected to be an appropriate scalar empirical descriptor for OPV3 and similar systems [28], since it reflects changes of the ionization constant for benzoic acid upon para-substitution. However, being empirical it is not readily available on demand [29], and also physical insight will be missed in this approach. There are many quantum chemical descriptors correlating with σ_p [27,30–32]. We need to determine one which best fits the stated goals, namely: be easy to calculate and straightforward to measure (to be not specific to calculation method) as well as have direct relation to electronic changes in an extended π -conjugated host molecule. Existing studies in this direction are rather limited. For example, in Ref. [23] a simple formula for predicting the dipole moment of donor-bridge-acceptor systems is proposed based on electronegativity and polarizability of the donor and acceptor; however, in the original formulation it is not applicable to a one-side functionalization, predicting zero dipole.

A close inspection of the molecule shown in Fig. 1 suggests that multiple elementary descriptors are needed to describe electronic density changes upon functionalization, which cause the observed modification of optoelectronic properties. Indeed, the lowest optically active excited state of an oligo(p-phenylene vinylene) is attributed to the $\pi - \pi^*$ transition [5]. Therefore the energies of π -HOMO and π -LUMO of the functional group, or any other orbitals resonant with the frontier orbitals of the host molecule, determine the changes in the electronic properties of the molecule upon functionalization. Also, since the functional group is attached through a σ -bond, the energies of the corresponding atomic orbitals determine charge redistribution along the bond. Additionally, the π - and σ -couplings between the attached group and the host molecule influence the amplitude of the changes. Therefore, physical quantities correlating with global charge redistribution across the bridging bond should be proper descriptors of electronic properties, in full accordance with previous studies [31,29,30].

The practical aspect of the present investigation is to put a solid quantitative basis for the above speculations. In a broad context, understanding of relationships between properties of a composite molecule and its fragments is an important tool for rational design of materials such as, for example, used in organic solar cells [33–35].

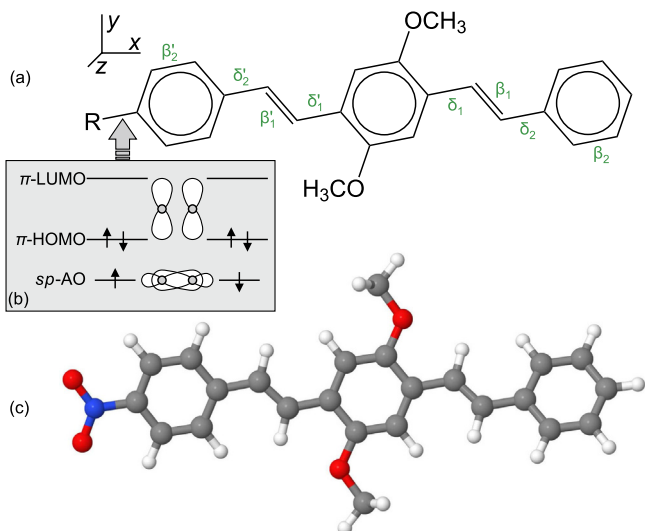


Fig. 1. (a) Functionalized oligo(p-phenylene vinylene) molecule. Available experimental data [2] are for $R = \text{H}, \text{Me}, \text{Br}, \text{NH}_2, \text{COOH}, \text{NO}_2$. (b) Essential molecular orbitals bridging the functional group and the host molecule. (c) Calculated geometry for NO_2 -functionalized molecule (NO₂-OPV3).

The paper is organized as follows. In the next section we discuss the computational methodology. Then we determine the proper molecular descriptor of electronic properties, followed by a theoretical analysis of the descriptor and electronic properties of a functionalized molecule. Finally we present and discuss our results of Density Functional Theory (DFT) calculations for ground, charged (cation/anion), and excited states. We rationalize every notable change in structural and electronic properties of a molecule upon functionalization. Also we compare performance of different computational methods to the available experimental data. Cross-references to [Supporting Information](#) have prefix "S".

2. Computational methodology

2.1. DFT calculations

Due to a large size of the studied molecules, the most appropriate theoretical tool for studying their properties is DFT and TDDFT (Time Dependent Density Functional Theory). Since the choice of the density functional is critical, different functionals are applied here. In particular for conjugated molecules the use of hybrid functionals is almost imperative [36]. Among the hybrids we test three different kinds of functionals: B3LYP [37,38], CAM-B3LYP [39], and ω B97X [40], see their brief description in [Table S10 \(Supporting Information\)](#). The first one is the most commonly used for organic molecules [36,41]. The last one is the long-range corrected functional: it is free of the self-interaction error. The CAM-B3LYP is a compromise between the established performance of B3LYP for a large class of molecules and the ever-increasing evidence of B3LYP failure due to its wrong long-range asymptotics. Hence, we use the CAM-B3LYP functional as default. For the studied molecules, it best fits the Koopman's theorem [42,43], [Table 4](#).

All calculations are performed with 6-31G^{**} basis set. Other basis sets are selectively considered for comparison with a detailed report given in [Section S14](#). This includes 6-31G and 6-31G^{*}, which together with 6-31G^{**} are known to provide good description of molecular energies and geometries [36,41]. Because most of the results for 6-31G^{**} and 6-31G^{*} sets are visually indistinguishable, their comparison is given in [Supporting Information](#). Other same-size basis sets considered are DGDZVP2 [44], Def2SVP [45], and cc-pVDZ as implemented in Gaussian [46]. Among them, the more commonly used cc-pVDZ is compared in the main text, whereas results for the other two sets are given in [Section S14](#).

The available experimental data were measured in a solution. To model the electrostatic effects of a solvent we use the CPCM conductor-like polarizable continuum model [47–49]. All the experimental data are also compared to the results for the PCM solvation model [47]; negligible difference from the CPCM calculations is observed. To consider nonelectrostatic solvation effects we use SMD model (as implemented in Gaussian 09 program [50,51]), which is parametrized for ground state calculations only [51,52].

Absorption and emission spectra are calculated for molecular geometries optimized in ground and excited states, respectively. Spectra are represented as vertical excitations through the set of transition energies and corresponding oscillator strengths. To match the experimental spectral profile (see [Fig. S12](#)), the obtained spectral lines are broadened with the Gaussian function. Because of the highly anharmonic potential energy surface (PES) for dihedrals, vibrationally resolved spectra are not calculated. The influence of a solvent is taken into account in both linear response (LR) [53] and state specific (SS) [54] approaches.

Charged states and electronic excitations are characterized by natural orbitals (NO) and natural transition orbitals (NTO) [55], respectively, which can be directly compared with molecular

orbitals (MO) of the neutral molecule in its ground state. Geometry optimization of charged and excited states is carried out starting from the optimized geometry of the ground state. All the calculations are performed in the Gaussian 09 program, Revision D.01 [50].

2.2. Analysis of the geometry

Backbone of OPV3 molecules consists of three benzene rings connected through vinyl chains. The resulting structure is highly flexible, and multiple conformations are possible. In order to find the most energetically favorable conformation, molecular dynamic simulation for all the molecules is carried out. TINKER package [56] with MM3 force field [57] is applied. Calculations are performed at room temperature, for 100 ps. A 360-degree rotation of the benzene rings and the interconnecting vinyl groups is observed. A few conformations within 0.2 eV energy range are obtained through optimization of molecular dynamics snapshots (first by MM3 and then by CAM-B3LYP). These conformations differ by the dihedrals at vinyl chains and the orientation OMe groups. In particular, the four lowest-energy conformations of H-OPV3 molecule differs by dihedrals only, with the energy difference between them less than 25 meV. The lowest conformation is globally twisted as in pure p-phenylene vinylene oligomers [58]. For NO₂-OPV3 only this configuration of dihedrals is observed. Conformations with rotated OMe groups start to appear at 0.1 eV. Electronic properties of various conformations differ insignificantly. In particular, the calculated peak positions of the absorption spectra differ by less than 0.05 eV. That is why only the lowest energy conformation is studied here (it is shown in Fig. 1).

Two geometrical parameters of conjugated polymers are very sensitive to changes in electronic density (and thus to the choice of the density functional [59]): bond length alternation between single and double bonds (BLA) [5,10], and dihedrals at single bonds [24]. Each vinyl group has one BLA and two dihedrals associated with it. In the excited or charged (cationic or anionic) states there are nonzero BLAs associated with phenyl rings. All these geometrical parameters used in the present work are shown in fig. 1a. In particular β_1 , shown near the double bond, is the difference between the half-sum of the lengths of the adjacent single bonds and the length of the double bond. The other three BLAs are defined in the same way. Parameter δ_1 , shown near the single bond, is the dihedral created by this bond and two adjacent bonds such that its value is closer to zero rather than to 180°. The other three dihedrals are defined in the same way, so that, for example, if all the dihedrals have the same sign then the whole molecule is twisted in one direction.

2.3. Analysis of experimental UV-vis absorption and photoluminescence spectra

Experimental UV-vis absorption spectra [2] measured in the wavelength bins as a function $I(\lambda)$ such that $\int I(\lambda) d\lambda$ counts the absorbed photons. This function is converted to the transition spectral density by the formula $f(E) \sim I(\lambda)\lambda^5$, where $E = 2\pi\hbar c/\lambda$. Then the first peak of $f(E)$ is fitted by the spectral density of a single quantum mode

$$f(E) = \frac{A}{\sqrt{2\pi\sigma^2}} \sum_{n=0}^{\infty} \frac{S_Q^n}{n!} \exp\left[-\frac{(E - E_C - E_Q n)^2}{2\sigma^2}\right], \quad (1)$$

here $A \equiv \int f(E) dE$ is the normalization constant, σ is the linewidth due to vibrational (classical modes) and inhomogeneous broadening, $E_Q \equiv \hbar\omega_Q$ and S_Q are the energy and Huang-Rhys factor of the quantum mode [60,8], and $E_C \equiv E_{\text{vert}} - S_Q E_Q$, where E_{vert} is the vertical transition energy. The same approach is used for treating

photoluminescence spectra, in this case $f(E) \sim I(\lambda)\lambda^5$. Technical details are given in Section S3 and thus estimated parameters are listed in Table S3.

2.4. Molecular descriptor and theoretical analysis of functionalization

Following the above introductory notes, several descriptors are tested theoretically using a set of 24 functional groups listed in Table S1. All the descriptors are based on easy to calculate properties of these groups (radicals or hydrogen passivated) and of functionalized phenyl (model system), namely, HOMO/LUMO energies and dipole moment. Hammett σ_p parameter is included as a reference. After identifying a set of descriptors providing the best statistical fit, a single descriptor is chosen for analysis of experimental data and DFT calculations of functionalized OPV3, in particular as horizontal axis in figures and leading column in tables.

To provide a physical insight into the functionalization, we use a variant of molecular orbital (MO) theory [61] based on localized MO (Kohn-Sham orbitals). In this approach we obtain two sets of MOs fully separated between two molecular fragments connected via a single bond, plus a pair of bonding and antibonding MOs corresponding to that bond. Technically, to get localized MOs we use natural bond orbital (NBO) analysis [62] as implemented in Gaussian 09 program [50]. Here the choice of localization method is not critical, while NBO is an appropriate approach for separating the bridging σ -bonding and anti-bonding MOs from the rest of MOs well localized on one of the two molecular fragments. Interfragment orbital interactions are considered within the second order perturbation theory [62,61,63]. In particular, charge transfer is calculated by the formula $\Delta n = 2t^2/\Delta\varepsilon^2$, where t and $\Delta\varepsilon$ are electron transfer integral and energy difference between a pair of interacting MOs. The total interfragment charge transfer calculated in our approach lies in between the values calculated from Mulliken and natural charges. Other details including wave-function and energy of localized MOs as well as list of strongest orbital interactions are given in Section S8 and Supplementary files. A more transparent though less accurate analysis based on semiempirical PM6 calculations [64,65] is given in Section S7.

3. Results and discussion

3.1. Molecular descriptor

Out of several descriptors considered, two show good statistical correlations. The first one is the electronegativity of the model system (functional group attached to phenyl). For the sake of computational efficiency we will use a relevant quantity, $\chi = -(E_{\text{HOMO}} + E_{\text{LUMO}})/2$, which differs from $(\text{IP} + \text{EA})/2$ for the studied molecules by tens of meV (see Fig. S20). The second is the relative dipole moment of the model system, δd_{\parallel} , which is the difference between dipole moments of the model system (d_{\parallel}) and hydrogen passivated functional group projected along the bridging bond and centered at this bond for charged species. The results of correlation analysis of these descriptors is given in Table 1 and Fig. 2. Both electronegativity and relative dipole moment as well as Hammett σ_p constant can be used as descriptors of electronic properties for R-OPV3 system. Of them we will use the relative dipole moment since it calculable and best correlates with empirical σ_p .

Importantly, both electronegativity and dipole moment, being scalar descriptors calculated for the model system, can be represented through multiple descriptors of the functional group itself. For electronegativity it is obvious [61], for dipole moment it is demonstrated in Section S6. In development of this idea, in Table 2 we have collected values of the descriptors and some results of MO

Table 1

Statistical analysis of correlations between descriptors and properties of functionalized OPV3 in terms of the coefficient of determination R^2 for the test set of 24 molecules listed in Table S1. In “neutral” subset charged species are excluded, in “small” subset extended π -conjugated molecules are excluded (Vi, Ph, Th, Py). All correlations are linear except for the last two properties where quadratic fit is used. See also the correlation plots in Fig. 2.

Property	Subset	σ_p	δd_{\parallel}	d_{\parallel}	χ
σ_p	Full	1	.93	.32	.68
σ_p	Neutral	1	.92	.57	.87
σ_p	Small	1	.95	.85	.88
Dipole moment	Neutral	.72	.75	.97	.79
IP	Neutral	.86	.87	.81	.85
EA	Neutral	.84	.86	.66	.95
Excitation energy	Small	.83	.89	.52	.85
Solvatochromic shift	Small	.67	.74	.38	.86

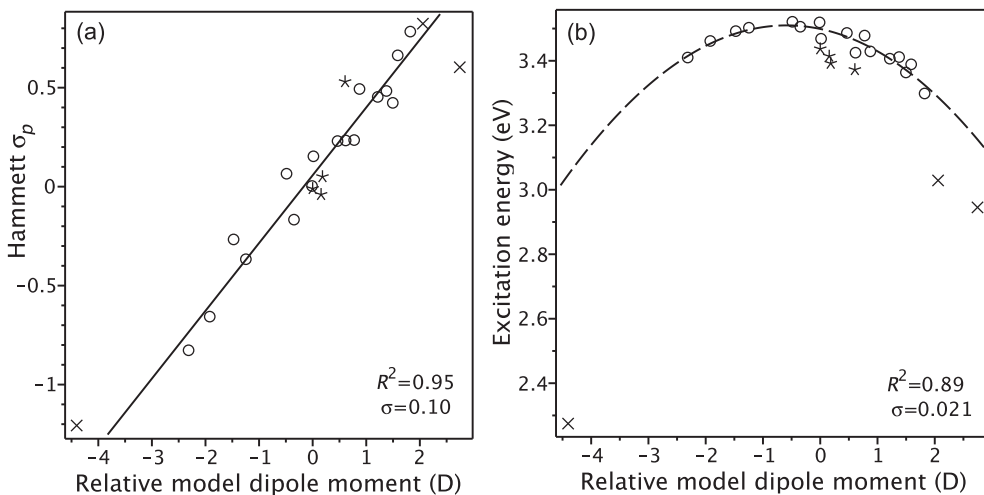


Fig. 2. Correlation plots between the relative model dipole moment δd_{\parallel} and (a) empirical Hammett σ_p constant, (b) calculated energy of the first excited state of functionalized OPV3 molecule (quadratic fit is used). The charged species are marked by cross, extended π -conjugated systems are marked by asterisk, the rest of the molecules are used in the statistical fit and are marked by circle. The standard deviation for residues is denoted by σ . Other correlation plots are given in Fig. S3.

analysis of several representative model systems including the six groups with available experimental data in R-OPV3 molecule. The main independent degrees of freedom are values of charge transfer through the bridging σ -bond, Δn^{σ} , and between π -systems of the functional group and phenyl, Δn^{π} . Several combinations of the sign and amount of transfer along these two channels are possible, composing different kinds of functionalization indistinguishable when using a scalar descriptor.

3.2. Electronic structure of the ground state

Frontier molecular orbitals of all the considered molecules belong to the π -conjugated system. HOMO and LUMO for all the functional groups studied in Ref. [2] are shown in Fig. 3a. The wave-function pattern on the host molecule is essentially the same

for all the HOMOs and all the LUMOs, justifying the use of the perturbation theory in the theoretical analysis. The global deformation of the frontier orbitals is mainly due to redistribution of the electronic density. It correlates well with the x -component of the electric dipole moment due to the electrostatics argument: a positive moment draws HOMO to the right and LUMO to the left. The correlation of the dipole moment with the descriptor δd_{\parallel} is illustrated in Fig. 4. The same trends are observed for the shifts of the IP/EA upon functionalization as shown in Fig. 5a.

To understand how functionalization changes the electronic properties of the ground state, we consider each functional group listed in Fig. 1 individually. In particular, NH_2 has no π -LUMO (see Fig. S9). Therefore the π -electrons are drawn in one direction: from the HOMO of NH_2 to the LUMO of the host molecule (see also Table 2). Yet there is a reverse charge flow within the σ -bond

Table 2

Descriptors and results of fragment MO analysis of the studied functional groups attached to phenyl (model system), with BH_2 and hypothetical planar- PH_2 added to discussion. Here $\Delta\epsilon$ is the HOMO energy upshift (+) or LUMO downshift (-) relative to benzene and Δn is the charge transfer from functional group to phenyl with superscript σ denoting through-bond transfer and π denoting dominant donor-acceptor transfer between π -MOs.

Group	σ_p	δd_{\parallel} (D)	$\delta\chi$ (eV)	$\Delta\epsilon$ (eV)	Δn^{π} (e)	Δn^{σ} (e)	Δn (e)
p- PH_2		-0.23	-0.92	+2.0	+0.13	+0.05	+0.12
NH_2	-0.66	-1.91	-0.76	+1.2	+0.13	-0.14	+0.05
Me	-0.17	-0.34	-0.17	+0.2	+0.02	0.00	+0.03
H	0	0	0	0	0	+0.11	+0.11
Br	0.23	0.79	0.14	+0.6	+0.05	-0.10	-0.01
COOH	0.45	1.23	0.88	-1.1	-0.07	-0.01	-0.01
BH_2		1.66	1.13	-1.8	-0.12	+0.13	-0.07
NO_2	0.78	1.83	1.69	-1.6	-0.06	-0.20	-0.18

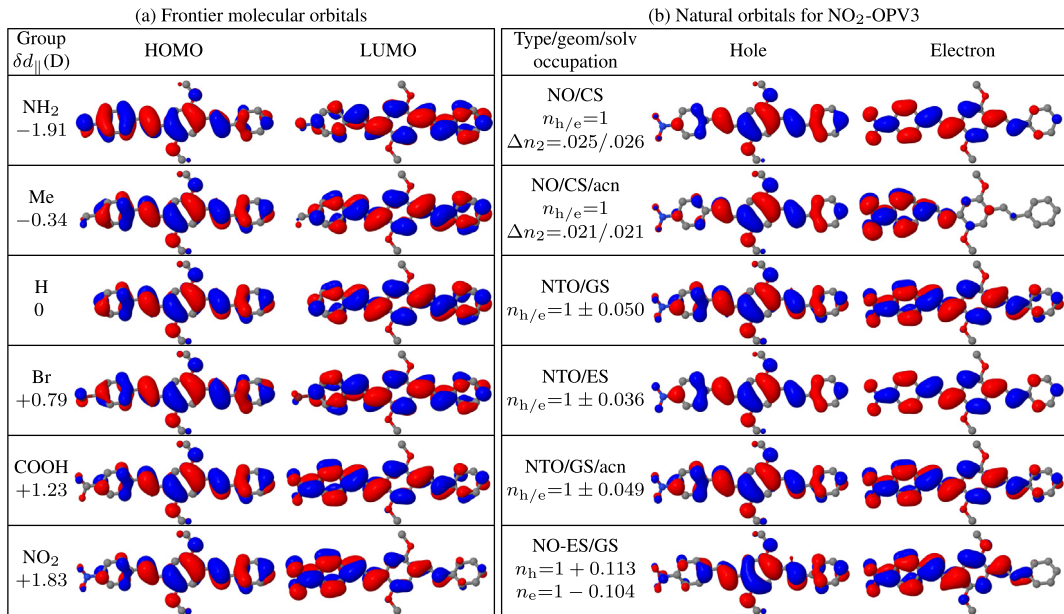


Fig. 3. (a) HOMO and LUMO in vacuum. Molecules are sorted by the descriptor δd_{\parallel} . (b) Comparison of different natural orbitals for NO₂-OPV3 molecule. Here GS/CS/ES means the state at which the geometry is optimized: G = Ground, C = Charged (cation for hole, anion for electron), E = Excited; NO-ES means NO for excited state density; $n_{h/e}$ is the occupation of the frontier orbitals; Δn_2 is the deviation of the occupation of the sub-frontier orbitals from 0 or 2. Calculations are performed in vacuo unless a solvent is specified (acn = acetonitrile). See also Section S9 for the same set of orbitals calculated for different functional groups and density functionals.

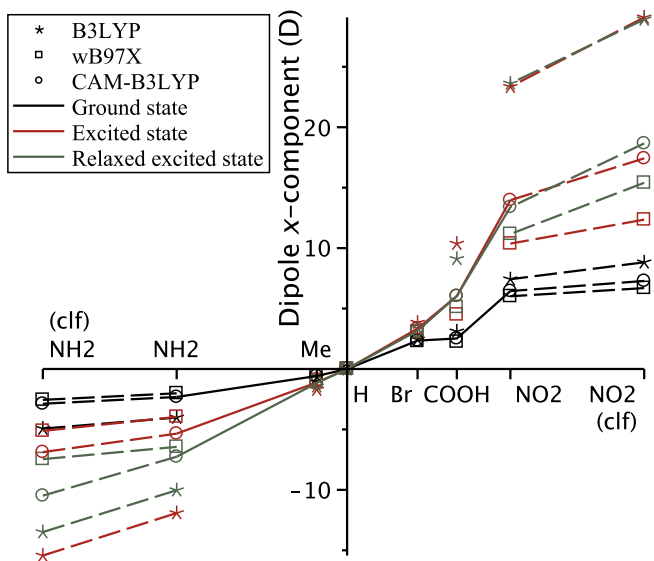


Fig. 4. Calculated dipole moments in vacuo and in chloroform (clf). Here only x-component is shown, see Fig. S23 for the absolute values. On the abscissa the value of δd_{\parallel} of the functional group is plotted except for the leftmost and rightmost tickmarks.

because the nitrogen in NH₂ is more electronegative than the carbon in the phenyl. The net charge balance is close to zero, but because the π -system is delocalized, a large net dipole moment is directed toward the amino group.

The HOMO of the molecule (the first row in Fig. 3a) is the anti-bonding superposition of the nitrogen's p_z -orbital and the HOMO of the host molecule (the third row in Fig. 3a), deformed by the net electric field of the molecule. Because the π -LUMO is absent on NH₂, the LUMO of the host molecule hybridizes with the nitrogen's p_z -orbital which is the HOMO of NH₂. Both the HOMO and the LUMO combinations are antibonding with the large π -coupling (see t_{π} in Table S4), resulting in the strong upshift of the energies

of these orbitals relative to H-OPV3 case. The LUMO shift is smaller than the HOMO shift because the composing orbitals are out of resonance. The overall downshift of MOs due to the increased attractive potential of the combined fragments downscale the upshifts to the numbers shown in Fig. 5a.

Bromine is isovalent with NH₂. However the bromine atom is much larger than the nitrogen leading to a much weaker π -coupling. This results in a small charge transfer within the π -system. This can be seen for the LUMO of the Br-OPV3 molecule: it has zero weight on the bromine (see Fig. 3a). Also, both HOMO and LUMO on the host molecule are visually identical to those of the hydrogen-ended molecule. Therefore the dipole moment is determined mainly by the charge redistribution within the σ -bond: being more electronegative the bromine pulls on the electronic density (see also Table 2).

The case of Me is more intricate because the π -orbitals hybridize with the rest of the orbitals through the sp^3 -carbon. But because the formal π -electronegativities of Me and Ph are comparable, the charge distribution is determined mainly by the σ -bond. This results in a small dipole directed towards the methyl group. The HOMO and LUMO levels of the host molecule lie well inside the π -gap of the hydrogen passivated Me. Therefore HOMO and LUMO are only slightly perturbed by the methyl group, as we observe in Fig. 3a.

The HOMO of the NO₂ group has zero weight on the nitrogen. Therefore the π -electrons are drawn from the HOMO of the host molecule to the LUMO of the NO₂. The charge flow within the bridging σ -bond has the same direction. This charge redistribution, together with the large co-aligned dipole moment of the NO₂ group alone, results in a huge dipole of the NO₂-OPV3 molecule. The HOMO is only slightly perturbed because of zero weight of the fragment HOMO on the nitrogen, see Fig. S7. Its energy downshift is due to the increased attractive potential of the combined fragments. The LUMO is the bonding combination of the LUMOs of the fragments deformed by the net electric field of the molecule. That is why a substantial downshift of the LUMO energy is observed in Fig. 5a. COOH differs from the NO₂ only quantitatively due to absence of charge transfer through σ -bond (see Table 2).

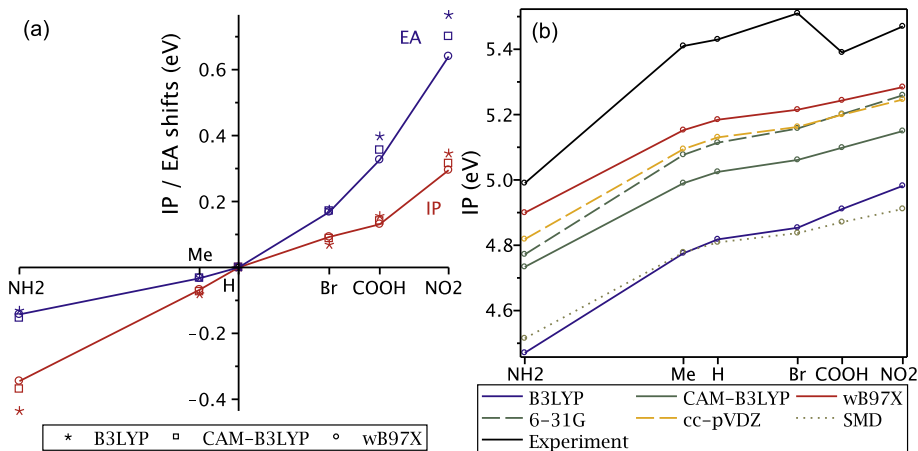


Fig. 5. (a) IP/EA shifts (in vacuo) relative to H-OPV3. (b) Experimental (cyclic voltammetry in acetonitrile) vs. predicted IP. The abscissa tickmarks correspond to values of δd_{\parallel} of the functional groups.

Overall, changes in electronic properties upon functionalization are determined by an interplay of charge transfer through σ -bond and π -system and correlate well with the proposed descriptors in full accordance with Table 2.

3.3. Structural properties of the ground state

The changes in the electronic properties described above are reflected in the structural changes. The most sensitive geometrical parameters are BLAs and dihedrals. The driving force for BLA is the charge density wave (bond order wave) [5]. For a vinyl group, the HOMO is localized on double bonds, whereas the LUMO is localized on single bonds (see Fig. 3a for MO wave-functions). Therefore if the electronic density is drawn from the HOMO or towards the LUMO, the BLA β_1 (or β'_1) decreases. This robust trend is clearly observed in Fig. 6a: functionalization destroys the perfect “half-filling” of the conjugated systems and both β_1 and β'_1 decrease.

There is also an important BLA associated with a phenyl ring: β_2 (or β'_2). In the ground state of H-OPV3 molecule $\beta_2 = 0.007 \text{ \AA}$. The rules for this BLA are opposite to those for β_1 : it increases with the population of the phenyl's LUMO or depopulation of phenyl's HOMO in full correspondence with the wave-function pattern (Fig. 3a) related to a pronounced Raman-active mode (Fig. S17) [10]. Therefore joining two phenyl rings leads to partial occupation/deoccupation of their LUMOs/HOMOs resulting in a positive β_2 for H-OPV3. For the same reason functionalization further increases this BLA up to $\beta'_2 = 0.016 \text{ \AA}$ for NH₂-OPV3.

The case of dihedrals is more intricate. The driving force planarizing dihedrals is the π -conjugation. That is why a vinyl group itself is almost flat, whereas its single bond links are often nonplanar. Therefore a strengthening of a single bond planarizes the dihedral if other relevant forces, e.g. steric interactions, remain unchanged. Consequently, dihedrals usually decrease upon functionalization, in full correspondence with DFT calculations in Fig. 6b.

3.4. Charged (cationic and anionic) states

The natural orbital analysis of NO₂-OPV3 anion, see Fig. 3b, shows that an extra electron occupying LUMO does not change this orbital in vacuum (electron NO \sim LUMO). In a polar solvent the electron NO is largely deformed by a self-consistent field of the solvent and the solute. The nature of this deformation is the same as for the corresponding LUMO: the solvent reaction field screens out electrostatic interactions thus allowing for larger shift of the electron density towards the electronegative amino group. The trends in the hole NO are qualitatively the same (hole NO \sim HOMO). Therefore the analysis of HOMO/LUMO changes upon functionalization made for the ground neutral state is valid for the corresponding NO of the charged molecule.

The geometry of a charged state is nearly planar due to the same effect as discussed above for explaining Fig. 6b: when an electron is placed at the π -LUMO or removed from the π -HOMO the bond order wave is suppressed, thus strengthening single

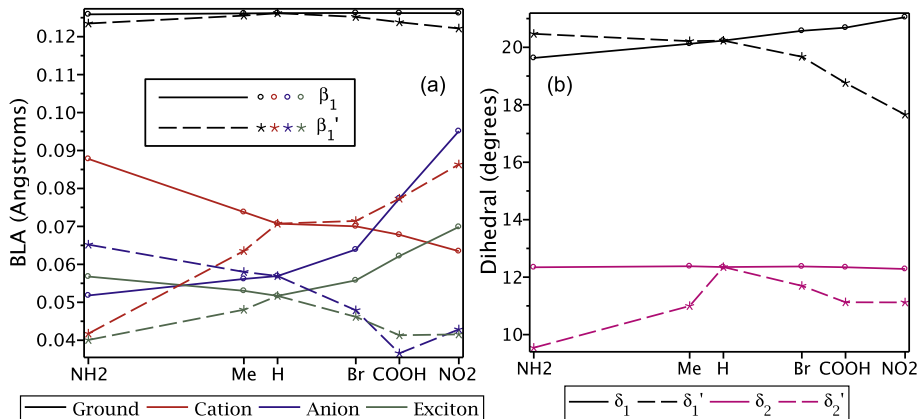


Fig. 6. Calculated geometrical parameters: (a) BLA for the two vinyl groups for four different relaxed states; (b) ground state geometry dihedrals. See Fig. 1 for notations.

bonds. This results in a decrease of all the dihedrals as well as the vinyl BLAs β_1 and β'_1 , see Fig. 6a. The dependence of these BLAs on the functional group follows the redistribution of the extra charge, so that the sum $\beta_1 + \beta'_1$ is nearly constant. For example, the COOH group of anion draws the negative extra charge, increasing the electronic density on the single bonds of the left vinyl group (see Fig. 3a), and thus decreasing the β'_1 . At the same time this redistribution increases the β_1 .

The case of NO₂-OPV3 anion is special: here the electronic density is substantially drawn out of OPV3 towards NO₂ (even in the ground state the sum of natural charges [62] on NO₂ is -0.3). As a result, β'_1 does not follow the monotonic trend in Fig. 6a (and Fig. S17).

Finally, we compare the IP measured by the cyclic voltammetry [2] with the calculated values, see Fig. 5b. The comparison shows the overall agreement between experiment and theory, except for Br-OPV3 which abnormally high value of oxidation potential requires an additional experimental investigation.

3.5. Excited states and UV-vis absorption

Experimental UV-vis absorption spectra show a well-resolved first absorption band followed by a less prominent second band [2]. Simulated spectra fully reproduce this picture as well as the overall spectral shape, see Fig. S12. TDDFT calculations attribute the first band to a single electronic transition with the large oscillator strength (1.6–1.9), while analysis of NTOs identifies it as HOMO to LUMO $\pi - \pi^*$ transition [2]. In what follows we will focus on this transition, common for light emitting conjugated polymers [5].

The shift of the first excitation energy upon functionalization is shown in Fig. 7a. The dependence on the functional group is well reproduced by TDDFT calculations and correlates with δd_{\parallel} descriptor. This dependence can be understood from Fig. 5a (IP/EA), because the optical gap for the considered system has linear correlation with the charge gap, see Fig. S3.

In homogeneous π -conjugated systems, such as H-OPV3, the few-atoms-averaged electronic density of the HOMO is the same as of the LUMO [5], so that the average density does not change significantly upon the HOMO–LUMO excitation. In contrast, for polar R-OPV3 molecules with essential redistribution of the electronic density between frontier MOs of the functional group and the host molecule the electronic density changes dramatically upon the HOMO–LUMO excitation resulting in a pronounced

solvatochromism [66,2,3]. The above changes can be traced by the electric dipole moment shown in Fig. 4. According to this figure for NH₂, COOH, NO₂ we observe a large dipole in the ground state as well as its large change upon excitation, whereas for Me and Br the change is much smaller compared to the value of the ground state dipole. This fact is easy to understand by the MO analysis: the π -system of the host molecule is undisturbed by Br or Me because of a small π -coupling (Br) or non-resonant conditions (Me).

Finally, we compare the calculated vibronic couplings with the results of a single quantum mode fit to the experimental absorption spectra. The latter give the energy of the quantum mode in the range of 0.17–0.20 eV, and the Huang–Rhys factor in the range of 0.7–1. As we already mentioned the highly anharmonic PES for dihedrals as well as the strong mode coupling between these librations and BLA-changing modes prevent a quantitative vibronic analysis based on the harmonic expansion of PES around the ground state using the default CAM-B3LYP density functional. Therefore we use B3LYP functional, for which the ground state geometry is planar. Also, B3LYP gives correct vibronic progression for OPV2 (stilbene) and OPV5, slightly underestimating the vibronic couplings [9]. The calculations for H-OPV3 (see Fig. S15) show the group of strongly coupled quantum modes in the range of 0.15–0.21 eV with the total Huang–Rhys factor 0.7. That is fully consistent with the experimental data.

3.6. Relaxed exciton and fluorescence

All the molecules studied in Ref. [2] are fluorescent in a dilute solution, which is attributed to the emission from the lowest excited singlet [2]. The next excited state is dark but is upshifted by more than 0.5 eV. In particular, for NO₂-OPV3 this state corresponds to the excitation fully localized on the functional group. The nature of the lowest excited state does not change upon geometry relaxation from the ground state, compare for example NTO/GS and NTO/ES of NO₂-OPV3 in Fig. 3b. For this reason, instead of discussing emission energy, it is more informative to consider Stokes shift defined as the difference between vertical excitation and deexcitation energies for the ground and excited state geometries respectively. Both calculated and measured Stokes shifts show weak dependence on functional group without a clear pattern, see Fig. 7b.

The geometry of the relaxed excited state is planar; the vinyl BLAs are much smaller than in the ground state geometry, see

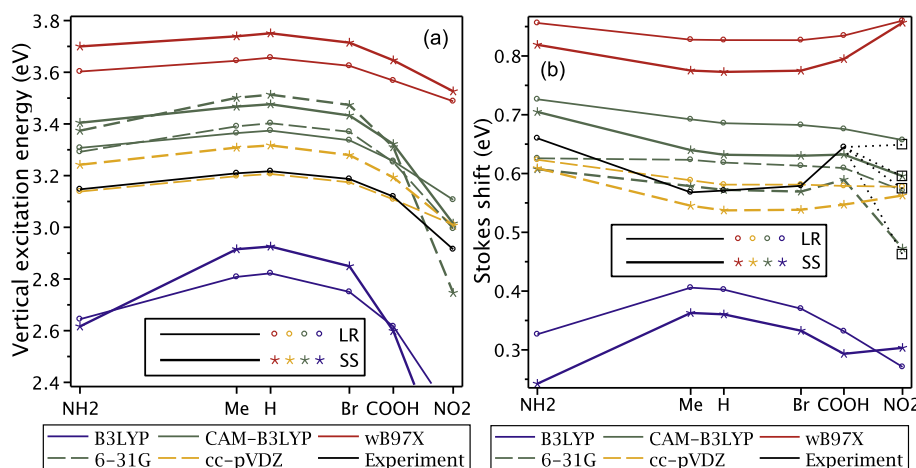


Fig. 7. (a) Experimental (UV-vis absorption in chloroform) vs. predicted first vertical excitation energy. (b) Stokes shifts (in chloroform). The fluorescence spectra for NO₂ have poor reproducibility due to intermolecular aggregation, the data from four different measurements are marked by the boxes.

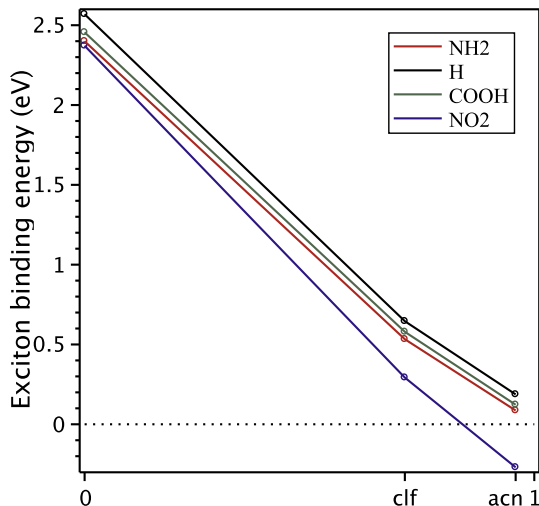


Fig. 8. Calculated exciton binding energy with relaxed geometries for all the states. The solvents are represented via their reaction field factor $(\epsilon - 1)/(\epsilon + 1/2)$, where ϵ is the static dielectric constant. Abbreviations: clf = chloroform, acn = acetonitrile.

Fig. 6a. These trends are identical to those for the charged states. In fact, BLAs for the exciton in **Fig. 6a** is a superposition of BLAs for the charged states (see also **Fig. S17**). The large geometrical relaxation results in large Stokes shifts. The analysis of the experimental spectra (see **Table S3**) shows that half of the Stokes shift is due to a quantum mode. This mode is ubiquitous for conjugated molecules and involves collective C–C stretching in a pattern similar to BLA [8]. Another half is due to low-frequency modes including librations.

In addition to changing excitation energy, functionalization changes also the transition dipole, especially pronounced upon charge separation. In particular, the mentioned partial charge transfer in NO₂-OPV3 anion is also observed for the first excited state. Indeed, the corresponding hole NO (the last row in **Fig. 3b**) changes dramatically on the left six atoms, adopting the shape of NO₂ LUMO. This implies that the wave-function is a superposition of the pure HOMO–LUMO excitation ($n_{h/e} = 1/1$) and pure charge transfer state ($n_{h/e} = 2/0$). In addition to a partial intramolecular charge transfer, for polar molecules in polar solvents an intermolecular charge transfer is energetically favorable, according to the total energy calculations presented in **Fig. 8**. This results in a strong quenching of photoluminescence upon the solute aggregation [2,3,67].

Overall, the nature of the lowest excited state of OPV3 molecule does not change upon functionalization by π -closed shell groups. It is an interacting electron–hole pair [5]. Consequently, observed trends can be understood by modification of HOMO, LUMO, and electron–hole interaction between them. As a result we observe the same parabola-shaped dependence of the excitation energy upon $\delta d_{||}$ as for the charge gap (IP–EA).

3.7. Two-sided functionalization

Two-sided functionalization gives more flexibility in tailoring molecular properties. We consider a set of R-OPV3-R' molecules, where the second functional group, R', is attached to the rightmost carbon in **Fig. 1**. There are two basic options: push–pull (R = acceptor, R' = donor) and symmetric (R = R') functionalization. In the first case, see **Table 3**, properties of R-OPV3-R' molecule combine the properties of R-OPV3 and OPV3-R' molecules additively [24], that is for a property P the following identity holds: $P(R - OPV3 - R') \approx P(R - OPV3) + P(OPV3 - R') - P(OPV3)$. In the symmetric case the additivity holds only for IP and dipole moments (zero by symmetry). The other properties depend on the LUMO energy, which does not change additively upon the attachment of the second NO₂. **3b** provides the explanation: the electron density of the LUMO is heavily depleted on the rightmost ring of NO₂-OPV3 molecule, to which the second NO₂ is attached.

Note that NO₂ group can be twisted in excited and negatively charged states [68]. This effect is not observed for molecules studied here. In particular, for NO₂-OPV3-NH₂ the twisted geometry is stationary but is 0.8 eV higher in energy than the planar one.

3.8. Methods assessment

Using available experimental data we assess the performance of different density functionals, basis sets, and solvation models. First, we discuss density functionals. The calculated BLAs and dihedrals for H-OPV3 are given in **Table 4**. Because the geometry for the studied molecules has not been measured experimentally, we mention published experimental data for vinyl BLAs and dihedrals in pure oligo and poly(p-phenylene vinylenes). In a crystal the experimental values for BLA are 0.134–0.144 Å for OPV2 [69], 0.18–0.27 Å for OPV5 [70]. Dihedrals in crystals of oligomers prefer buckling geometry (phenyl rings are coplanar) due to geometrical constraints, with angles ranging from 0 to 7° [69,70]. In polymers, the distribution of dihedrals is much broader [71]. In a gas phase the observed dihedrals for stilbene have flat distribution with angles of up to 30° [72].

Based on **Table 4**, IPs in **Fig. 5b**, excitation energies in **Fig. 7a**, and Stokes shifts in **Fig. 7b**, we conclude that CAM-B3LYP and ω B97X functionals give reasonable geometrical parameters and dependencies on the functional group for the whole set of data, whereas B3LYP is rather inaccurate for all the datasets. The errors correlate with the deviation from the Koopman's theorem identity $IP + E_{HOMO} = 0$ [42,43,73] (see also **Fig. S18**). Interestingly, B3LYP gives very good estimates of the lowest excitation energy for phenylene vinylene family of molecules [11,9], however the observed functional group dependence (see **Fig. 7**) is very inaccurate.

The other computed properties (no experiment available) show the same trend: B3LYP results differ significantly from those calculated by the two long-range corrected functionals. In particular, for the exciton binding energy both CAM-B3LYP and ω B97X give nearly the same values within 0.05 eV, whereas B3LYP estimates

Table 3

Two-sided functionalization. Here E_{bind}^{acn} is the exciton binding energy in acetonitrile, ΔE_{exc}^{acn} is the solvatochromic shift (LR approach); all other quantities are calculated in vacuum including the Stokes shift ΔE_{abs}^{emi} and the x-component of the dipole moment in the geometrically relaxed excited state d_x^{exc} .

R	R'	EA (eV)	IP (eV)	E_{exc} (eV)	ΔE_{abs}^{emi} (eV)	E_{bind}^{acn} (eV)	ΔE_{exc}^{acn} (eV)	d_x (D)	d_x^{exc} (D)
H	H	0.46	6.21	3.52	0.59	0.32	0.13	0	0
H	NH ₂	0.31	5.84	3.46	0.61	0.24	0.14	-2.3	-7.3
NO ₂	H	1.16	6.52	3.30	0.54	-0.12	0.20	+6.4	+13.4
NO ₂	NH ₂	1.00	6.10	3.20	0.55	-0.28	0.20	+9.0	+21.2
By additivity		1.01	6.16	3.24	0.56	-0.21	0.21	+8.8	+20.6
NO ₂	NO ₂	1.55	6.86	3.23	0.53	0.22	0.23	0	0
By additivity		1.86	6.84	3.08	0.48	-0.57	0.27	0	0

Table 4

Dependence of calculated properties of H-OPV3 molecule on density functional and basis set: geometrical parameters BLA β_1 and dihedral δ_1 (in vacuum), deviations from experiment for IP in acetonitrile and excitation energy in chloroform, deviations from the Koopman's identities $\delta\text{IP} = \text{IP} + E_{\text{HOMO}}$ and $\delta\chi = (\text{IP} + \text{EA} + E_{\text{HOMO}} + E_{\text{LUMO}})/2$ (ground state geometry in vacuum).

Method	β_1 (Å)	δ_1 (°)	ΔIP (eV)	ΔE_{exc} (eV)	δIP (eV)	$\delta\chi$ (meV)
B3LYP	0.112	14	-0.61	-0.40	1.24	10
CAM-B3LYP	0.126	20	-0.41	0.16	0.29	-8
ω B97X	0.133	24	-0.25	0.44	-0.46	-29
6-31G	0.122	13	-0.32	0.19	0.31	-4
cc-pVDZ	0.125	11	-0.30	-0.01	0.27	-8
DGDZVP2	0.125	0	-0.15	-0.06	0.27	-9
Def2SVP	0.124	0	-0.23	-0.01	0.28	-7

are higher by up to 0.5 eV. The largest discrepancy between different density functionals is for electric dipole moments in the excited state, see Fig. 4. It originates from the overestimated by B3LYP charge transfer character of this state [74]. The effect is especially pronounced for NO₂-OPV3 molecule: CAM-B3LYP predicts a partial charge transfer to NO₂ group due to HOMO-LUMO transition ($n_{\text{h/e}} = 1.1/0.9$ in the last row of Fig. 3), whereas B3LYP predicts a larger charge transfer due to HOMO-LUMO mixing ($n_{\text{h/e}} = 1.6/0.4$ with both natural orbitals containing NO₂ LUMO as shown in Table S9).

The sensitivity of the calculated data to the basis set is not as dramatic as to the density functional: the differences in all the computed energies are within 0.1–0.15 eV from the median, see also Section S14. More importantly, the relative differences (with respect to functional group) are even smaller except for 6-31G basis. Consequently, no preference can be given in our study to any of considered same-size basis sets from the point of view of accuracy. The difference between 6-31G* and 6-31G** is inessential, so that the use of the smaller one is reasonable for π -conjugated molecules with aliphatic side-chains commonly present in solution-processed materials [1]. The use of the smaller 6-31G basis is acceptable for preliminary calculations and for large molecules when basis set size is critical. The dependence of δIP of H-OPV3 molecule at cc-pVDZ geometry on basis set size is smooth and weak: cc-pVDZ 0.273, cc-pVTZ 0.247, cc-pVQZ 0.240, cc-pV5Z 0.235 (all in eV).

Among polarizable continuum solvation models, CPCM gives essentially the same computed values for our dataset as more sophisticated PCM (in the present paper we do not study the dependence on solvent). The SMD model should be more accurate in predicting IP, because it considers nonelectrostatic effects more accurately, which are expected to be significant for the considered molecules. Indeed they are large: more than 0.2 eV, see Fig. 5b. Surprisingly, SMD corrections only increase the discrepancy with the measured IP.

The excited state solvation is more intricate because SS and LR approaches describe different solvent effects: the former thoroughly treats electrostatic effects, whereas the latter partially takes into account both electrostatic and dispersive interactions [75]. Based on the UV-vis absorption spectra (Fig. 7a) it is hard to judge which approach is better at reproducing the experimental data. For emission, LR approach is strictly speaking not applicable, hence the comparison of Stokes shifts (Fig. 7b) gives a clear preference to SS treatment. However, if computational time matters, LR approach can be used for calculating emission spectra because the difference with SS results is less than 0.1 eV, that is within the accuracy of current DFT methods.

4. Conclusions

In summary, a comprehensive (TD) DFT study supplemented by in-depth MO analysis is performed to understand and quantify

structural and electronic changes in oligo(p-phenylene vinylene) molecules upon functionalization. Our calculations are in a good agreement with the experimental data [2]. In particular, the use of a higher level of theoretical analysis compared to Ref. [2] allows us to confirm the suggested there assignment of the high-energy photoluminescence band to the fluorescence of individual molecules (the other band is attributed to aggregates [2]).

Two scalar quantum chemical descriptors are shown to correlate with optoelectronic properties of functionalized OPV3: electronegativity and relative dipole moment of a minimal π -closed-shell fragment of the OPV3 molecule to which the functional group is attached. Since that fragment is phenyl in a para-substitution pattern, both descriptors correlate linearly with the empirical Hammett σ_p constant. The theoretical analysis shows that these scalar descriptors defined for the model system, can be represented via multiple descriptors of the functional group itself. It is naturally to expect that this rule is applied for other extended π -conjugated systems, namely: a scalar quantum chemical descriptor is to be searched not for a functional group itself but for a minimal π -closed-shell fragment containing the group.

Using a set of available experimental data, an assessment of density functionals, small basis sets, and solvation models is made. The performance of the density functionals correlates well with the calculated IP + HOMO and EA + LUMO, the former should be zero for an exact DFT. In practice this means that at least two different density functionals with the opposite values of IP + HOMO and EA + LUMO should be used in calculations. Then the difference in the computed values can serve as a measure of uncertainty of these values.

All considered small basis sets show nearly the same dependence of calculated properties upon functionalization, so that the smaller one, 6-31G*, can be reliably used for calculation of optoelectronic properties of extended π -conjugated molecules.

The comparison of SMD solvation model with PCM/CPCM models shows that nonelectrostatic solvent effects are large (0.2 eV). But, surprisingly, the corrections of SMD model increase the difference between the calculated and measured IP (cyclic voltammetry). For excitations, LR and SS approaches differ by less than 0.1 eV. For absorption no preference can be given to any of them.

Acknowledgements

We acknowledge support of Directed Research and Development Fund, Center for Integrated Nanotechnology (CINT) and Center for Nonlinear Studies (CNLS) at Los Alamos National Laboratory (LANL) – United States. LANL is operated by Los Alamos National Security, LLC, for the National Nuclear Security Administration of the U.S. Department of Energy under contract DE-AC52-06NA25396.

This research used computing facilities of Skolkovo Institute of Science and Technology.

Appendix A. Supplementary data

Supplementary data associated with this article can be found, in the online version, at <http://dx.doi.org/10.1016/j.chemphys.2016.09.009>.

References

- [1] H. Klauk, *Organic Electronics II: More Materials and Applications*, Wiley, 2012.
- [2] Y.I. Park, C.-Y. Kuo, J.S. Martinez, Y.-S. Park, O. Postupna, A. Zhugayevych, S. Kim, J. Park, S. Tretiak, H.-L. Wang, Tailored electronic structure and optical properties of conjugated systems through aggregates and dipole-dipole interactions, *ACS Appl. Mater. Interfaces* 5 (2013) 4685–4695, <http://dx.doi.org/10.1021/am400766w>.
- [3] Y.I. Park, O. Postupna, A. Zhugayevych, H. Shin, Y.-S. Park, B. Kim, H.-J. Yen, P. Cheruku, J.S. Martinez, J.W. Park, S. Tretiak, H.-L. Wang, A new pH sensitive fluorescent and white light emissive material through controlled intermolecular charge transfer, *Chem. Sci.* 6 (2015) 789–797, <http://dx.doi.org/10.1039/C4SC01911C>.
- [4] M. Pope, C. Swenberg, *Electronic Processes in Organic Crystals and Polymers*, Oxford University Press, 1999.
- [5] W. Barford, *Electronic and Optical Properties of Conjugated Polymers*, Oxford University Press, 2005.
- [6] T. Skotheim, J. Reynolds, *Handbook of Conducting Polymers*, CRC Press, 2007.
- [7] W. Salaneck, R. Friend, J. Bredas, Electronic structure of conjugated polymers: consequences of electron-lattice coupling, *Phys. Rep.* 319 (1999) 231–251, [http://dx.doi.org/10.1016/S0370-1573\(99\)00052-6](http://dx.doi.org/10.1016/S0370-1573(99)00052-6).
- [8] S. Karabunliev, M. Baumgarten, E.R. Bittner, K. Mullen, Rigorous frank-condon absorption and emission spectra of conjugated oligomers from quantum chemistry, *J. Chem. Phys.* 113 (2000) 11372–11381, <http://dx.doi.org/10.1063/1.1328067>.
- [9] M. Dierksen, S. Grimme, The vibronic structure of electronic absorption spectra of large molecules: a time-dependent density functional study on the influence of exact hartree-fock exchange, *J. Phys. Chem. A* 108 (2004) 10225–10237, <http://dx.doi.org/10.1021/jp047289h>.
- [10] G. Zerbi, *Vibrational Spectroscopy of Conducting Polymers: Theory and Perspective*, in: *Handbook of Vibrational Spectroscopy*, Wiley, 2006, <http://dx.doi.org/10.1002/9780470027325.s8920>.
- [11] A. Masunov, S. Tretiak, Prediction of two-photon absorption properties for organic chromophores using time-dependent density-functional theory, *J. Phys. Chem. B* 108 (2004) 899–907, <http://dx.doi.org/10.1021/jp036513k>.
- [12] F. Terenziani, C. Katan, E. Badaeva, S. Tretiak, M. Blanchard-Desce, Enhanced two-photon absorption of organic chromophores: Theoretical and experimental assessments, *Adv. Mater.* 20 (2008) 4641–4678, <http://dx.doi.org/10.1002/adma.200800402>.
- [13] V.M. Geskin, F.C. Grozema, L.D.A. Siebbeles, D. Beljonne, J.L. Bredas, J. Cornil, Impact of the computational method on the geometric and electronic properties of oligo(phenylene vinylene) radical cations, *J. Phys. Chem. B* 109 (2005) 20237–20243, <http://dx.doi.org/10.1021/jp0519417>.
- [14] J. Gierschner, J. Cornil, H.-J. Egelhaaf, Optical bandgaps of pi-conjugated organic materials at the polymer limit: experiment and theory, *Adv. Mater.* 19 (2007) 173–191, <http://dx.doi.org/10.1002/adma.200600277>.
- [15] S. Tretiak, V. Chernyak, S. Mukamel, Origin, scaling, and saturation of second order polarizabilities in donor/acceptor polyenes, *Chem. Phys. Lett.* 287 (1998) 75–82, [http://dx.doi.org/10.1016/S0009-2614\(98\)00156-0](http://dx.doi.org/10.1016/S0009-2614(98)00156-0).
- [16] C. Wu, S. Tretiak, V.Y. Chernyak, Excited states and optical response of a donor-acceptor substituted polyene: a td-dft study, *Chem. Phys. Lett.* 433 (2007) 305–311, <http://dx.doi.org/10.1016/j.cplett.2006.11.069>.
- [17] H. Li, C. Wu, S.V. Malinin, S. Tretiak, V.Y. Chernyak, Excited states of donor and acceptor substituted conjugated oligomers: a perspective from the exciton scattering approach, *J. Phys. Chem. Lett.* 1 (2010) 3396–3400, <http://dx.doi.org/10.1021/jz1013533>.
- [18] M. Hanack, B. Behnisch, H. Hackl, P. Martinez-Ruiz, K.-H. Schweikart, Influence of the cyano-group on the optical properties of oligomeric ppv-derivatives, *Thin Solid Films* 417 (2002) 26–31, [http://dx.doi.org/10.1016/S0040-6090\(02\)00591-6](http://dx.doi.org/10.1016/S0040-6090(02)00591-6).
- [19] B. Strehmel, A.M. Sarker, H. Detert, The influence of sigma and pi acceptors on two-photon absorption and solvatochromism of dipolar and quadrupolar unsaturated organic compounds, *ChemPhysChem* 4 (2003) 249–259, <http://dx.doi.org/10.1002/cphc.200390041>.
- [20] H.Y. Woo, B. Liu, B. Kohler, D. Korystov, A. Mikhailovsky, G.C. Bazan, Solvent effects on the two-photon absorption of distyrylbenzene chromophores, *J. Am. Chem. Soc.* 127 (2005) 14721–14729, <http://dx.doi.org/10.1021/ja052906g>.
- [21] H. Meier, B. Muhling, J. Gerold, D. Jacob, A. Oehlhof, Push-pull oligomers with 2,2-dicyanovinyl groups as electron acceptors, *Eur. J. Org. Chem.* 2007 (2007) 625–631, <http://dx.doi.org/10.1002/ejoc.200600704>.
- [22] S.J.K. Pond, M. Rumi, M.D. Levin, T.C. Parker, D. Beljonne, M.W. Day, J.-L. Bredas, S.R. Marder, J.W. Perry, One- and two-photon spectroscopy of donor-acceptor-donor distyrylbenzene derivatives: effect of cyano substitution and distortion from planarity, *J. Phys. Chem. A* 106 (2002) 11470–11480, <http://dx.doi.org/10.1021/jp0267104>.
- [23] J.Y. Lee, K.S. Kim, B.J. Mhin, Intramolecular charge transfer of pi-conjugated push-pull systems in terms of polarizability and electronegativity, *J. Chem. Phys.* 115 (2001) 9484–9489, <http://dx.doi.org/10.1063/1.1413986>.
- [24] V. Ediz, J.L. Lee, B.A. Armitage, D. Yaron, Molecular engineering of torsional potentials in fluorogenic dyes via electronic substituent effects, *J. Phys. Chem. A* 112 (2008) 9692–9701, <http://dx.doi.org/10.1021/jp805546s>.
- [25] R. Todeschini, V. Consonni, *Molecular Descriptors for Chemoinformatics*, Wiley, 2009.
- [26] C. Hansch, A. Leo, R.W. Taft, A survey of hammett substituent constants and resonance and field parameters, *Chem. Rev.* 91 (1991) 165–195, <http://dx.doi.org/10.1021/cr00002a004>.
- [27] G.C. Shields, P.G. Seybold, Computational Approaches for the Prediction of pKa Values, CRC Press (2014), <http://dx.doi.org/10.1201/b16128>.
- [28] A. Irfan, A.G. Al-Sehemi, M.S. Al-Assiri, Push-pull effect on the electronic, optical and charge transport properties of the benzo[2,3-b]thiophene derivatives as efficient multifunctional materials, *Comput. Theor. Chem.* 1031 (2014) 76–82, <http://dx.doi.org/10.1016/j.comptc.2013.12.027>.
- [29] P. Ertl, Simple quantum chemical parameters as an alternative to the hammett sigma constants in qsar studies, *Quant. Struct.-Act. Relat.* 16 (1997) 377–382, <http://dx.doi.org/10.1002/qsar.19970160505>.
- [30] T. Papp, L. Kollar, T. Kegl, Employment of quantum chemical descriptors for hammett constants: revision suggested for the acetoxy substituent, *Chem. Phys. Lett.* 588 (2013) 51–56, <http://dx.doi.org/10.1016/j.cplett.2013.10.017>.
- [31] T.M. Krygowski, N. Sadlej-Sosnowska, Towards physical interpretation of hammett constants: charge transferred between active regions of substituents and a functional group, *Struct. Chem.* 22 (2011) 17–22, <http://dx.doi.org/10.1007/s11224-010-9676-9>.
- [32] Y. Takahata, A.D.S. Marques, Accurate core-electron binding energy shifts from density functional theory, *J. Electron. Spectrosc. Relat. Phenom.* 178–179 (2010) 80–87, <http://dx.doi.org/10.1016/j.jelspec.2009.03.018>.
- [33] Z.B. Henson, G.C. Welch, T. van der Poll, G.C. Bazan, Pyridalthiadiazole-based narrow band gap chromophores, *J. Am. Chem. Soc.* 134 (2012) 3766–3779, <http://dx.doi.org/10.1021/ja209331y>.
- [34] J.E. Coughlin, A. Zhugayevych, I. Ronald, C. Bakus, T.S. van der Poll, G.C. Welch, S.J. Teat, G.C. Bazan, S. Tretiak, A combined experimental and theoretical study of conformational preferences of molecular semiconductors, *J. Phys. Chem. C* 118 (2014) 15610–15623, <http://dx.doi.org/10.1021/jp506172a>.
- [35] A. Zhugayevych, S. Tretiak, Theoretical description of structural and electronic properties of organic photovoltaic materials, *Annu. Rev. Phys. Chem.* 66 (2015) 305–330, <http://dx.doi.org/10.1146/annurev-physchem-040214-121440>.
- [36] C. Cramer, *Essentials of Computational Chemistry: Theories and Models*, Wiley, 2004.
- [37] A.D. Becke, Density-functional thermochemistry. III. the role of exact exchange, *J. Chem. Phys.* 98 (1993) 5648–5652, <http://dx.doi.org/10.1063/1.464913>.
- [38] P.J. Stephens, F.J. Devlin, C.F. Chabalowski, M.J. Frisch, Ab initio calculation of vibrational absorption and circular dichroism spectra using density functional force fields, *J. Phys. Chem.* 98 (1994) 11623–11627, <http://dx.doi.org/10.1021/j100096a001>.
- [39] T. Yanai, D.P. Tew, N.C. Handy, A new hybrid exchange-correlation functional using the Coulomb-attenuating method (CAM-B3LYP), *Chem. Phys. Lett.* 393 (2004) 51–57.
- [40] J.-D. Chai, M. Head-Gordon, Systematic optimization of long-range corrected hybrid density functionals, *J. Chem. Phys.* 128 (2008) 084106, <http://dx.doi.org/10.1063/1.2834918>.
- [41] Nist computational chemistry comparison and benchmark database, URL <http://cccbdb.nist.gov>.
- [42] J.P. Perdew, R.G. Parr, M. Levy, J.L. Balduz, Density-functional theory for fractional particle number: derivative discontinuities of the energy, *Phys. Rev. Lett.* 49 (1982) 1691–1694, <http://dx.doi.org/10.1103/PhysRevLett.49.1691>.
- [43] R. Baer, E. Livshits, U. Salzner, Tuned range-separated hybrids in density functional theory, *Annu. Rev. Phys. Chem.* 61 (2010) 85–109, <http://dx.doi.org/10.1146/annurev.physchem.012809.103321>.
- [44] N. Godbout, D.R. Salahub, J. Andzelm, E. Wimmer, Optimization of gaussian-type basis sets for local spin density functional calculations. Part I. Boron through neon, optimization technique and validation, *Can. J. Chem.* 70 (1992) 560–571, <http://dx.doi.org/10.1139/v92-079>.
- [45] F. Weigend, R. Ahlrichs, Balanced basis sets of split valence, triple zeta valence and quadruple zeta valence quality for H to RN: design and assessment of accuracy, *Phys. Chem. Chem. Phys.* 7 (2005) 3297–3305, <http://dx.doi.org/10.1039/B508541A>.
- [46] E.R. Davidson, Comment on comment on dunning's correlation-consistent basis sets, *Chem. Phys. Lett.* 260 (1996) 514–518, [http://dx.doi.org/10.1016/0009-2614\(96\)00917-7](http://dx.doi.org/10.1016/0009-2614(96)00917-7).
- [47] J. Tomasi, B. Mennucci, R. Cammi, Quantum mechanical continuum solvation models, *Chem. Rev.* 105 (2005) 2999–3094, <http://dx.doi.org/10.1021/cr9904009>.
- [48] M. Cossi, N. Rega, G. Scalmani, V. Barone, Energies, structures, and electronic properties of molecules in solution with the c-pcm solvation model, *J. Comput. Chem.* 24 (2003) 669–681, <http://dx.doi.org/10.1002/jcc.10189>.
- [49] Y. Takano, K.N. Houk, Benchmarking the conductor-like polarizable continuum model (cpcm) for aqueous solvation free energies of neutral and ionic organic molecules, *J. Chem. Theory Comput.* 1 (2005) 70–77, <http://dx.doi.org/10.1021/ct049977a>.
- [50] M.J. Frisch, G.W. Trucks, H.B. Schlegel, G.E. Scuseria, M.A. Robb, J.R. Cheeseman, G. Scalmani, V. Barone, B. Mennucci, G.A. Petersson, H. Nakatsuji, M. Caricato, X. Li, H.P. Izmaylov, A.F. Bloino, G. Zheng, J.L. Sonnenberg, M. Hada, M. Ehara, K. Toyota, R. Fukuda, J. Hasegawa, M. Ishida, T. Nakajima, Y. Honda, O. Kitao, H. Nakai, T. Vreven, J.A. Montgomery, Jr., J.E. Peralta, F. Ogliaro,

- M. Bearpark, J.J. Heyd, E. Brothers, K.N. Kudin, V.N. Staroverov, R. Kobayashi, J. Normand, K. Raghavachari, A. Rendell, J.C. Burant, S.S. Iyengar, J. Tomasi, M. Cossi, N. Rega, J.M. Millam, M. Klene, J.E. Knox, J.B. Cross, V. Bakken, C. Adamo, J. Jaramillo, R. Gomperts, R.E. Stratmann, O. Yazyev, A.J. Austin, R. Cammi, C. Pomelli, J.W. Ochterski, R.L. Martin, K. Morokuma, V.G. Zakrzewski, G.A. Voth, P. Salvador, J.J. Dannenberg, S. Dapprich, A.D. Daniels, Farkas, J.B. Foresman, J.V. Ortiz, J. Cioslowski, D.J. Fox, Gaussian 09 Revision A.1, gaussian Inc., Wallingford CT, 2009.
- [51] A.V. Marenich, C.J. Cramer, D.G. Truhlar, Universal solvation model based on solute electron density and on a continuum model of the solvent defined by the bulk dielectric constant and atomic surface tensions, *J. Phys. Chem. B* 113 (2009) 6378–6396, <http://dx.doi.org/10.1021/jp810292n>.
- [52] C.J. Cramer, D.G. Truhlar, Implicit solvation models: equilibria, structure, spectra, and dynamics, *Chem. Rev.* 99 (1999) 2161–2200, <http://dx.doi.org/10.1021/cr960149m>.
- [53] M. Cossi, V. Barone, Time-dependent density functional theory for molecules in liquid solutions, *J. Chem. Phys.* 115 (2001) 4708–4717, <http://dx.doi.org/10.1063/1.1394921>.
- [54] M. Cossi, V. Barone, Solvent effect on vertical electronic transitions by the polarizable continuum model, *J. Chem. Phys.* 112 (2000) 2427–2435, <http://dx.doi.org/10.1063/1.480808>.
- [55] R.L. Martin, Natural transition orbitals, *J. Chem. Phys.* 118 (2003) 4775–4777, <http://dx.doi.org/10.1063/1.1558471>.
- [56] J.W. Ponder, Tinker 6.2. URL <http://dasher.wustl.edu/tinker>.
- [57] N.L. Allinger, F. Li, L. Yan, J.C. Tai, Molecular mechanics (mm^3) calculations on conjugated hydrocarbons, *J. Comput. Chem.* 11 (1990) 868–895, <http://dx.doi.org/10.1002/jcc.540110709>.
- [58] J.B. Lagowski, Ab initio investigation of conformational and excitation energies of phenylene vinylene oligomers, *J. Mol. Struct. (Thoechem)* 589 (2002) 125–137, [http://dx.doi.org/10.1016/S0166-1280\(02\)00253-1](http://dx.doi.org/10.1016/S0166-1280(02)00253-1).
- [59] D. Jacquemin, C. Adamo, Bond length alternation of conjugated oligomers: wave function and DFT benchmarks, *J. Chem. Theory Comput.* 7 (2011) 369–376, <http://dx.doi.org/10.1021/ct1006532>.
- [60] K. Huang, A. Rhys, Theory of light absorption and non-radiative transitions in f-centres, *Proc. R. Soc. London, Ser. A* 204 (1950) 406–423, <http://dx.doi.org/10.1098/rspa.1950.0184>.
- [61] F. Jensen, *Introduction to Computational Chemistry*, Wiley, 2007.
- [62] F. Weinhold, C.R. Landis, *Discovering Chemistry with Natural Bond Orbitals*, Wiley, 2012.
- [63] A. Zhugayevych, V. Lubchenko, Electronic structure and the glass transition in pnictide and chalcogenide semiconductor alloys. I. The formation of the pp sigma-network, *J. Chem. Phys.* 133 (2010) 234503, <http://dx.doi.org/10.1063/1.3511707>.
- [64] J.J. Stewart, Optimization of parameters for semiempirical methods V: modification of nddo approximations and application to 70 elements, *J. Mol. Model.* 13 (2007) 1173–1213, <http://dx.doi.org/10.1007/s00894-007-0233-4>.
- [65] J.J.P. Stewart, Mopac 2009. URL <http://openmopac.net>.
- [66] C. Reichardt, T. Welton, *Solvents and Solvent Effects in Organic Chemistry*, Wiley, 2011.
- [67] S. Tretiak, A. Saxena, R.L. Martin, A.R. Bishop, Interchain electronic excitations in poly(phenylenevinylene) (ppv) aggregates, *J. Phys. Chem. B* 104 (2000) 7029–7037, <http://dx.doi.org/10.1021/jp000397t>.
- [68] G. Scalmani, M.J. Frisch, B. Mennucci, J. Tomasi, R. Cammi, V. Barone, Geometries and properties of excited states in the gas phase and in solution: theory and application of a time-dependent density functional theory polarizable continuum model, *J. Chem. Phys.* 124 (2006) 094107, <http://dx.doi.org/10.1063/1.2173258>.
- [69] J. Harada, K. Ogawa, X-ray diffraction analysis of nonequilibrium states in crystals: observation of an unstable conformer in flash-cooled crystals, *J. Am. Chem. Soc.* 126 (2004) 3539–3544, <http://dx.doi.org/10.1021/ja038203l>.
- [70] P.F. van Hütten, J. Wildeman, A. Meetsma, G. Hadzioannou, Molecular packing in unsubstituted semiconducting phenylenevinylene oligomer and polymer, *J. Am. Chem. Soc.* 121 (1999) 5910–5918, <http://dx.doi.org/10.1021/ja990934r>.
- [71] G. Mao, J.E. Fischer, F.E. Karasz, M.J. Winokur, Nonplanarity and ring torsion in poly(p-phenylene vinylene), a neutron-diffraction study, *J. Chem. Phys.* 98 (1993) 712–716, <http://dx.doi.org/10.1063/1.464616>.
- [72] P.D. Chowdary, T.J. Martinez, M. Gruebele, The vibrationally adiabatic torsional potential energy surface of trans-stilbene, *Chem. Phys. Lett.* 440 (2007) 7–11, <http://dx.doi.org/10.1016/j.cplett.2007.03.109>.
- [73] J. Autschbach, M. Srebro, Delocalization error and 'functional tuning' in kohn-sham calculations of molecular properties, *Acc. Chem. Res.* 47 (2014) 2592–2602, <http://dx.doi.org/10.1021/ar500171t>.
- [74] R.J. Magyar, S. Tretiak, Dependence of spurious charge-transfer excited states on orbital exchange in tddft: large molecules and clusters, *J. Chem. Theory Comput.* 3 (2007) 976–987, <http://dx.doi.org/10.1021/ct600282k>.
- [75] R. Improta, V. Barone, G. Scalmani, M.J. Frisch, A state-specific polarizable continuum model time dependent density functional theory method for excited state calculations in solution, *J. Chem. Phys.* 125 (2006) 054103, <http://dx.doi.org/10.1063/1.2222364>.

Supporting Information for Modification of Optoelectronic Properties of Conjugated Oligomers Due to Donor/Acceptor Functionalization: DFT Study

Andriy Zhugayevych, Olena Postupna, Hsing-Lin Wang, Sergei Tretiak

November 11, 2016

S1	List of functional groups	S2
S2	Correlation plots	S3
S3	Single quantum mode fit to transition spectral density	S5
S4	Experimental data	S6
S5	Perturbation theory for weakly interacting systems	S7
S6	Calculation of charge transfer for semiempirical Hamiltonian	S8
S7	Semiempirical analysis	S9
S8	Localized molecular orbitals analysis	S11
S9	Molecular and natural orbitals (basis set 6-31G)	S14
S10	UV-Vis absorption spectra	S19
S11	NTO analysis of the second absorption band	S20
S12	Vibronic couplings	S21
S13	Comparison of density functionals used in this work	S23
S14	Comparison of basis sets used in this work	S25
S15	Other figures and tables	S27

S1 List of functional groups

Group	s	Name	IP(eV)	EA(eV)	σ_p	δd_{\parallel} (D)	$\delta \chi$ (eV)
S ⁻	x	sulfur anion			-1.21	-4.39	-5.74
NMe ₂	o	dimethylamino radical	8.2		-0.83	-2.30	-1.01
NH ₂	e	amino radical	10.8	0.8	-0.66	-1.91	-0.76
OH	o	hydroxyl radical	13.0	1.8	-0.37	-1.23	-0.36
OMe	o	methoxy radical	10.7	1.6	-0.27	-1.46	-0.44
Me	e	methyl radical	9.8	0.1	-0.17	-0.29	-0.19
Vi	*	vinyl radical	8.3	0.7	-0.04	0.16	0.12
Ph	*	phenyl radical	8.3	1.1	-0.01	0.00	0.04
H	e	hydrogen	13.6	0.8	0.00	0.00	0.00
Th	*	2-thienyl	8.9		0.05	0.18	0.04
F	o	fluorine	17.4	3.4	0.06	-0.48	0.12
SH	o	thiol	10.4	2.3	0.15	0.03	-0.29
Cl	o	chlorine	13.0	3.6	0.23	0.48	0.20
CCH	o	ethynyl radical	11.6	3.0	0.23	0.63	0.23
Br	e	bromine	11.8	3.4	0.23	0.79	0.14
CHO	o	formyl radical	8.1	0.3	0.42	1.51	1.11
COOH	e	hydrocarboxyl radical	8.2	3.5	0.45	1.23	0.88
BF ₂	o	difluoroboron	9.4	2.1	0.48	1.39	0.85
NC	o	cyano radical	14.2	3.9	0.49	0.89	0.75
Py	*	2-pyrimidinyl	9.3		0.53	0.60	0.55
NH ₃ ⁺	x	ammoniumyl			0.60	2.76	4.76
CN	o	cyano radical	14.2	3.9	0.66	1.60	1.03
NO ₂	e	nitrogen dioxide	9.6	2.3	0.78	1.83	1.69
NMe ₃ ⁺	x	trimethylammonium cation			0.82	2.07	4.33
BH ₂	o	boron dihydride	9.8	0.2		1.66	1.13

Table S1: A set of functional groups used in statistical analysis of molecular descriptors. The column “s” corresponds to the symbol used in correlation plots, namely: x – ions, * – extended π -conjugated systems, o – all other groups, with “e” denoting those studied experimentally in [5]. Numerical data in the columns are experimental IP and EA [2], empirical Hammett σ_p parameter [1], and the two calculated quantum chemical descriptors: relative model dipole moment δd_{\parallel} and model electronegativity relative to benzene $\delta \chi$. Experimental EA for OMe is from Ref. [3], calculated EA for BH₂ is from Ref. [4]. Empty cells mean no available data.

Group	Conformation	ΔE (meV)	$\hbar\omega$ (meV)	δd_{\parallel} (D)	$\delta \chi$ (eV)
Me	staggered	0	+3.6	-0.29	-0.19
Me	eclipsed	0.6	-3.8	-0.34	-0.17
NH ₃ ⁺	staggered	0	+2.2	2.76	4.76
NH ₃ ⁺	eclipsed	0.2	-2.9	2.76	4.77
SH	eclipsed	0	+10.1	0.03	-0.29
SH	staggered	20	-8.3	0.59	0.36
PH ₂	relaxed	0	+5.1	0.66	0.32
PH ₂	opposite sides	0.2	-3.5	0.69	0.41
PH ₂	same side	23	-10.0	0.36	-0.09
NH ₂	nonplanar	0	30-60	-1.91	-0.76
NH ₂	planar	38	-53.3	-1.87	-0.94

Table S2: Conformational dependence of calculated descriptors for selected model systems (functional group attached to phenyl): low-energy zero-gradient conformations in vacuum are listed. Here ω is the frequency of the relevant vibrational mode (negative sign denotes imaginary frequency).

S2 Correlation plots

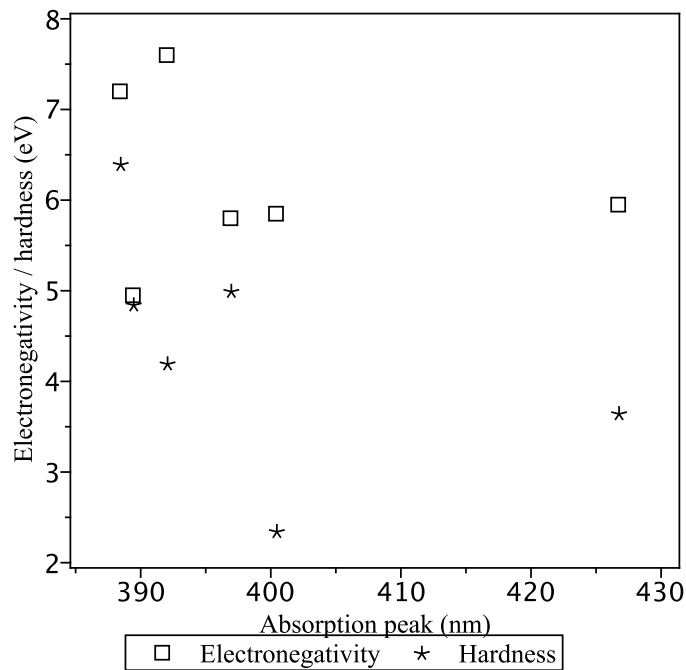


Figure S1: Correlation plot between the position of absorption peak, measured in chloroform solution for the six functional groups considered in Ref. [5], and electronegativity and chemical hardness of functional groups calculated from IP/EA as $(IP + EA)/2$ and $(IP - EA)/2$ respectively.

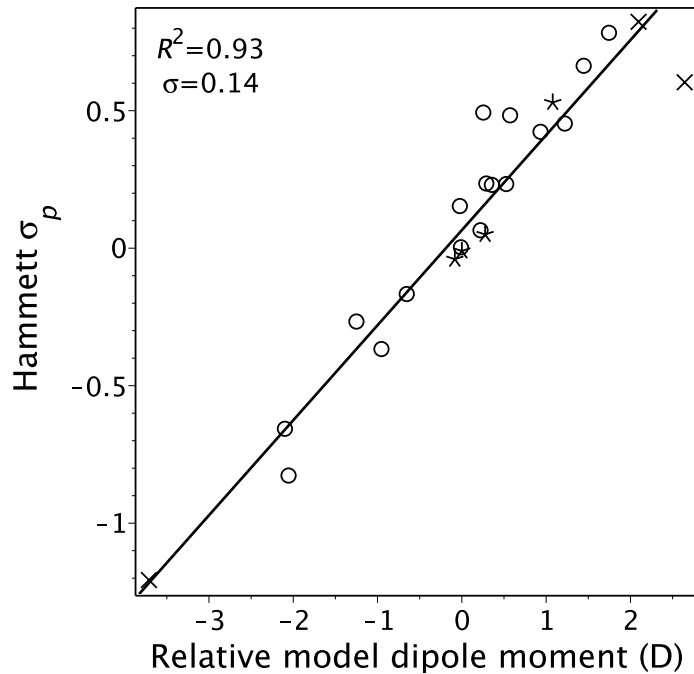


Figure S2: Correlation plot between relative model dipole moment calculated by semiempirical PM7 method and Hammett σ_p parameter for the test set from Table S1.

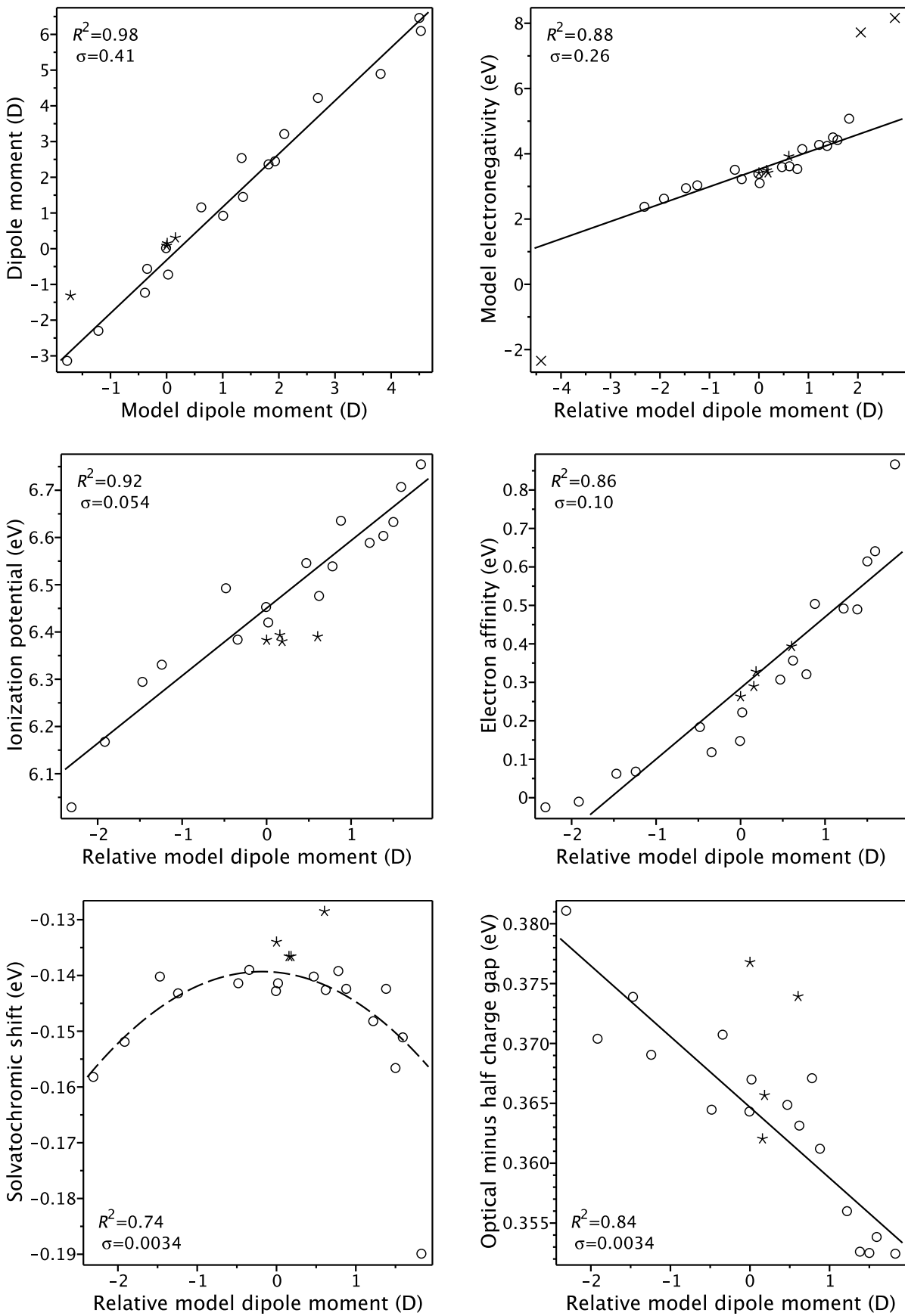


Figure S3: Correlation plots between relative model dipole moment and various descriptors and physical properties of R-OPV3. The solvatochromic shift is for chloroform, the corresponding statistical fit does not include NO_2 (the circle at lower right corner).

S3 Single quantum mode fit to transition spectral density

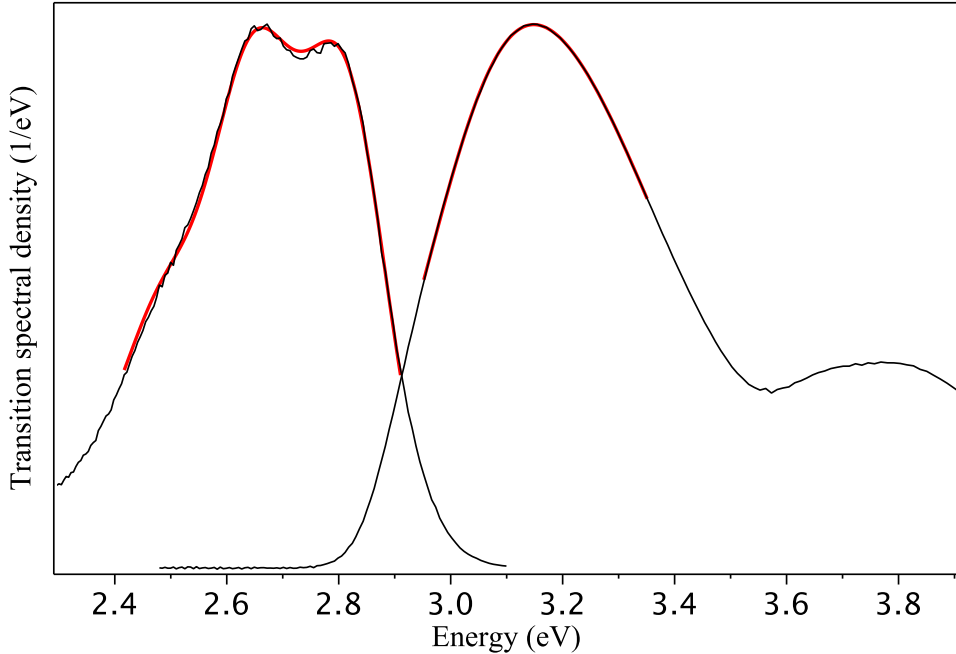


Figure S4: Experimental transition spectral density (amplitude normalized to 1) for emission (left black curve) and absorption (right black curve) of H-OPV3 in chloroform solution. Red curves are the single quantum mode fits.

For a given electronic transition, the transition spectral density (vibrational) is given by

$$f(E) = \sum_{nn'} \rho_n \langle n|n' \rangle^2 \delta(E - E_{nn'}), \quad (\text{S1})$$

where the indexes n and n' enumerate the initial and final vibrational states, respectively, ρ_n is the initial occupation of state n , $\langle n|n' \rangle$ is the vibrational overlap integral (Franck–Condon factor), and $E_{nn'}$ is the transition energy. For the displaced harmonic oscillator model with one quantum mode ($\rho_n = \delta_{n0}$) the transition spectral density is given by Eq. (1).

Experimental spectra are fitted by Eq. (1) using the least-squares method. Only three out of five parameters can be robustly estimated: A , E_{vert} , and $\sigma'^2 \equiv \sigma^2 + S_Q E_Q^2$, because they correspond to the normalization, mean value, and variance of the transition spectral density, respectively. These three moments cannot be computed in practice because tails of experimental spectra may contain other transitions. However, they can be estimated (as an initial guess) using the second order fit to the maximum with the following approximate identities:

$$f_{\max} = \frac{A}{\sqrt{2\pi\sigma'^2}}, \quad -\frac{f_{\max}}{f''_{\max}} = \sigma'^2, \quad E_{\max} = E_{\text{vert}} - \frac{S_Q E_Q}{2S_Q + 1}. \quad (\text{S2})$$

The computational algorithm as well as the working program can be found at the web-page <http://zhugayevych.me/maple/MolMod> (SingleQModeFit subroutine of Molecular Modeling package).

S4 Experimental data

Group	Solvent	λ_{\max} (nm)	E_{vert} (eV)	σ_E (eV)	$\hbar\omega_Q$ (eV)	S_Q
Absorption: Dependence on solvent						
NO ₂	thf	422.4(1)	2.947(5)	0.240(3)	0.20	0.9
NO ₂	tol	423.9(4)	2.944(3)	0.223(1)	0.17	1.4
NO ₂	clf	426.7(1)	2.915(4)	0.240(1)	0.19	1.0
NO ₂	clb	429.4(1)	2.901(8)	0.230(4)	0.18	1.1
NO ₂	dmso	430.2(1)	2.884(2)	0.254(1)	0.21	0.9
Absorption: Dependence on functional group						
H	clf	388.4(2)	3.217(3)	0.218(3)	0.20	0.7
Me	clf	389.4(2)	3.209(3)	0.216(2)	0.19	0.8
Br	clf	392.0(2)	3.187(3)	0.218(4)	0.20	0.8
NH ₂	clf	396.9(1)	3.147(6)	0.223(3)	0.20	0.8
COOH	clf	400.4(2)	3.119(4)	0.225(6)	0.20	0.7
NO ₂	clf	426.7(1)	2.915(4)	0.240(1)	0.19	1.0
Emission: Dependence on functional group						
H	clf	441.8(4)	2.646(6)	0.181(2)	0.16	1.0
Me	clf	442.2(4)	2.641(10)	0.182(13)	0.17	1.0
Br	clf	445.6(11)	2.608(6)	0.191(0)	0.17	1.0
NH ₂	clf	473.9(7)	2.487(2)	0.199(4)	0.15	1.3
COOH	clf	474.9(16)	2.474(2)	0.193(1)	0.16	1.2
NO ₂	clf	481.9(11)	2.453(2)	0.192(3)	0.15	1.3

Table S3: Processed experimental UV-Vis absorption and fluorescence data from Ref. [5]. Here λ_{\max} is the absorption/emission peak in the original wavelength scale estimated by a fourth-order polynomial fit to the raw data; E_{vert} , σ_E , $\hbar\omega_Q$, S_Q are the vertical transition energy, spectral width, energy and Huang–Rhys factor of the quantum mode, all estimated by the single quantum mode fit, see Section S3. The last digit uncertainty is the superposition of the statistical fitting error and the change upon expanding or contracting the fitting range (red curve in Fig. S4) by about 30%. The uncertainties of $\hbar\omega_Q$ and S_Q are comparable to the spread of their values across the table. The measurements are made in chloroform with the solute concentration 10^{-4} M for absorption and 10^{-6} M for emission. Abbreviations for solvents: clb=chlorobenzene, clf=chloroform, dmso=dimethylsulfoxide, thf=tetrahydrofuran, tol=toluene.

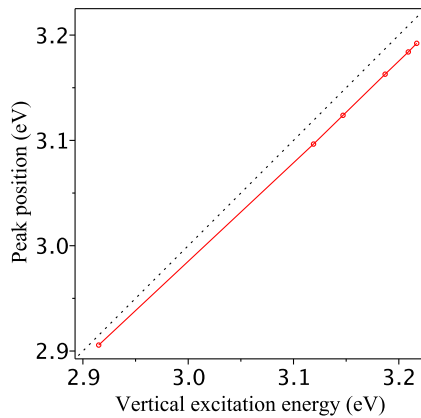


Figure S5: Vertical excitation energy E_{vert} versus peak position determined from λ_{\max} , see Table S3.

S5 Perturbation theory for weakly interacting systems

Here we provide the formulas of the perturbation theory (see e.g. Refs. [6–8]) used in the semiempirical analysis. In our approximation we have two weakly interacting systems (host molecule and functional group) with a nondiagonal perturbation (π -coupling). The small parameter is $2t_\pi/(E_{\text{LUMO}}^{\text{acceptor}} - E_{\text{HOMO}}^{\text{donor}})$, which is smaller than 1 for all the systems listed in Table S4.

Let the one-particle Hamiltonian be

$$\begin{pmatrix} H^A & V \\ V^\top & H^B \end{pmatrix}, \quad (\text{S3})$$

where V is the interaction matrix. Let ψ_n^A and E_n^A (ψ_m^B and E_m^B) be the unperturbed eigenfunctions and eigenvalues. The second order perturbation of the eigenelements of the system A is given by

$$\psi_n = \left(1 - \frac{1}{2} \sum_m^B \frac{|V_{mn}|^2}{E_{nm}^2} \right) \psi_n^A + \sum_m^B \frac{V_{mn}}{E_{nm}} \psi_m^B + \sum_{n' \neq n}^A \sum_m^B \frac{V_{mn}}{E_{nm}} \frac{V_{n'm}}{E_{nn'}} \psi_{n'}^A, \quad E_n = E_n^A + \sum_m^B \frac{|V_{mn}|^2}{E_{nm}}. \quad (\text{S4})$$

where $E_{nm} = E_n^A - E_m^B$ and $V_{mn} = \langle \psi_m^B | V | \psi_n^A \rangle$. For two multielectron systems, each represented by a single Slater determinant, the second order perturbation theory for the one-electron density matrix (per spin) reads

$$\begin{aligned} \rho = & \sum_n^{A_{\text{occ}}} \begin{pmatrix} |\psi_n^A\rangle\langle\psi_n^A| & 0 \\ 0 & 0 \end{pmatrix} + \sum_m^{B_{\text{occ}}} \begin{pmatrix} 0 & 0 \\ 0 & |\psi_m^B\rangle\langle\psi_m^B| \end{pmatrix} + \left\{ \sum_n^{A_{\text{occ}}} \sum_m^{B_{\text{uno}}} - \sum_n^{A_{\text{uno}}} \sum_m^{B_{\text{occ}}} \right\} \frac{V_{nm}}{E_{nm}} \begin{pmatrix} 0 & |\psi_n^A\rangle\langle\psi_m^B| \\ |\psi_m^B\rangle\langle\psi_n^A| & 0 \end{pmatrix} \\ & + \left\{ \sum_{n,n'}^{A_{\text{occ}}} \sum_m^{B_{\text{uno}}} - \sum_{n,n'}^{A_{\text{uno}}} \sum_m^{B_{\text{occ}}} \right\} \frac{V_{nm}}{E_{nm}} \frac{V_{mn'}}{E_{mn'}} \begin{pmatrix} |\psi_n^A\rangle\langle\psi_{n'}^A| & 0 \\ 0 & 0 \end{pmatrix} + \text{"the same for B"} \\ & + \left\{ \sum_n^{A_{\text{occ}}} \sum_{n'}^{A_{\text{uno}}} \sum_m^{B_{\text{uno}}} - \sum_n^{A_{\text{uno}}} \sum_{n'}^{A_{\text{occ}}} \sum_m^{B_{\text{occ}}} \right\} \frac{V_{nm}}{E_{nm}} \frac{V_{mn'}}{E_{nn'}} \begin{pmatrix} |\psi_n^A\rangle\langle\psi_{n'}^A| & 0 \\ 0 & 0 \end{pmatrix} + \text{"hermitean conjugated"} + \text{"the same for B"}, \end{aligned} \quad (\text{S5})$$

where “occ” and “uno” mean the sum over occupied and unoccupied levels respectively. For the two closed shell (paired spins) systems A and B, the charge redistribution between them is given by

$$\Delta n^A = 2 \sum_n^A (\rho_{nn} - \rho_{nn}^A) = -2 \left\{ \sum_n^{A_{\text{occ}}} \sum_m^{B_{\text{uno}}} - \sum_n^{A_{\text{uno}}} \sum_m^{B_{\text{occ}}} \right\} \frac{|V_{mn}|^2}{E_{nm}^2} \equiv -\Delta n^B. \quad (\text{S6})$$

The formula for the bond order [8] differs by the sign:

$$b^{AB} = 4 \left\{ \sum_n^{A_{\text{occ}}} \sum_m^{B_{\text{uno}}} + \sum_n^{A_{\text{uno}}} \sum_m^{B_{\text{occ}}} \right\} \frac{|V_{mn}|^2}{E_{nm}^2}. \quad (\text{S7})$$

Finally, for any one-particle operator d , its perturbation on the system A is given by

$$\begin{aligned} \Delta d^A = & 2 \sum_{nn'}^A (\rho_{nn'} - \rho_{nn'}^A) d_{n'n}^A \\ = & 2 \left\{ \sum_{n,n'}^{A_{\text{occ}}} \sum_m^{B_{\text{uno}}} - \sum_{n,n'}^{A_{\text{uno}}} \sum_m^{B_{\text{occ}}} \right\} \frac{V_{nm}}{E_{nm}} \frac{V_{mn'}}{E_{mn'}} d_{n'n}^A + 4\Re \left\{ \sum_n^{A_{\text{occ}}} \sum_{n'}^{A_{\text{uno}}} \sum_m^{B_{\text{uno}}} - \sum_n^{A_{\text{uno}}} \sum_{n'}^{A_{\text{occ}}} \sum_m^{B_{\text{occ}}} \right\} \frac{V_{nm}}{E_{nm}} \frac{V_{mn'}}{E_{nn'}} d_{n'n}^A, \end{aligned} \quad (\text{S8})$$

where $d_{n'n}^A = \langle \psi_{n'}^A | d | \psi_n^A \rangle$.

S6 Calculation of charge transfer for semiempirical Hamiltonian

For a composite A+B molecule we calculate the total number of electrons transferred from A to B, $\Delta n^B = -\Delta n^A$, and the x -component of the dipole, d , in the coordinate system of Fig. 1 with A fragment on the left. Other quantities of interest can be calculated using the same approach.

Note: all the transfer integrals are chosen to be positive; in this case all the on-site values of the lowest MO are positive; hence transfer integrals enter the molecular Hamiltonian with the negative sign in front of them.

Treatment of the σ -bond is straightforward:

$$\Delta n_\sigma^A = \frac{\varepsilon_\sigma^B - \varepsilon_\sigma^A}{\sqrt{(\varepsilon_\sigma^B - \varepsilon_\sigma^A)^2 + (2t_\sigma^{AB})^2}}, \quad t_\sigma^{AB} = \frac{t_\sigma^{AH} t_\sigma^{BH}}{t_\sigma^{HH}}, \quad \Delta d_\sigma = ea^{AB} \Delta n_\sigma^A, \quad a^{AB} = a^{AH} + a^{BH} - a^{HH}, \quad (\text{S9})$$

here a^{AB} is the estimated bond-length.

Before considering the whole π -system, MOs for some fragments should be provided, namely: phenyl in Fig. S6 and NO₂ in Fig. S7.

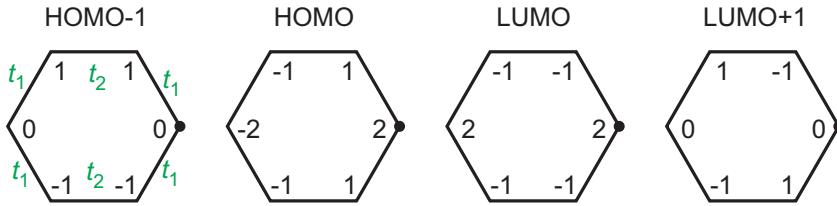


Figure S6: Frontier molecular orbitals of the distorted phenyl ring. The distortion pattern is indicated by the transfer integrals, and corresponds to the minimal symmetry breaking, which occurs in the molecules considered in the present paper. Numbers are the values of the unnormalized wave-function. The bridging atom is shown.

For the π -system, we use the second order perturbation theory over π -coupling t_π^{AB} . Using the formulas of Section S5 with $V_{mn} = -\psi_m^B t_\pi^{AB} \psi_n^A$, and taking only one HOMO ($n, m = 0$) and one LUMO ($n, m = 1$) per fragment, it is straightforward to derive the required formulas:

$$\Delta n_\pi^A = -\frac{1}{2} c_{AB}^2 + \frac{1}{2} c_{BA}^2, \quad b_\pi = c_{AB}^2 + c_{BA}^2, \quad (\text{S10})$$

$$\Delta d_\pi^A = -\frac{1}{2} c_{AB}^2 d_{00}^A + \frac{1}{2} c_{BA}^2 d_{11}^A + \left(c_{AB} \frac{2\psi_1^A t_\pi^{AB} \psi_1^B}{\varepsilon_{\pi 1}^A - \varepsilon_{\pi 0}^A} - c_{BA} \frac{2\psi_0^B t_\pi^{AB} \psi_0^A}{\varepsilon_{\pi 1}^A - \varepsilon_{\pi 0}^A} \right) d_{01}^A, \quad (\text{S11})$$

where

$$c_{AB} = \frac{2\psi_0^A t_\pi^{AB} \psi_1^B}{\varepsilon_{\pi 1}^B - \varepsilon_{\pi 0}^A}, \quad c_{BA} = \frac{2\psi_0^B t_\pi^{AB} \psi_1^A}{\varepsilon_{\pi 1}^A - \varepsilon_{\pi 0}^B}. \quad (\text{S12})$$

The x -component of the dipole is the sum of all the contributions:

$$d = d^A + d^B + \Delta d_\pi^A + \Delta d_\pi^B + ea\Delta n_\pi^A + \Delta d_\sigma, \quad (\text{S13})$$

where a is the distance between the reference points of the matrix elements $d_{nn'}^A$ and $d_{mm'}^B$.

Finally, we estimate the π -coupling in a self-consistent field of the redistributed electrons:

$$t_\pi^{AB} = \tilde{t}_\pi^{AB} + \rho_{AB} (t_\pi^{AB}) W, \quad (\text{S14})$$

where \tilde{t}_π^{AB} is the bare transfer integral¹ calculated using PM6 parametrization [9], ρ_{AB} is the element of the per-spin density matrix between the π -orbitals of the bridging atoms calculated by formula (S5), and W is the Coulomb interaction matrix element estimated as e^2/a^{AB} . Solving (S14) with respect to t_π^{AB} yields

$$t_\pi^{AB} = \tilde{t}_\pi^{AB} \left(1 - \left[\frac{(\psi_0^A \psi_1^B)^2}{\varepsilon_{\pi 1}^B - \varepsilon_{\pi 0}^A} + \frac{(\psi_0^B \psi_1^A)^2}{\varepsilon_{\pi 1}^A - \varepsilon_{\pi 0}^B} \right] \frac{e^2}{a^{AB}} \right)^{-1}. \quad (\text{S15})$$

¹See Ref. [10, formula 18]: $\tilde{t}_\pi^{AB} = S_{\pi\pi}^{AB}(a^{AB})(\beta_\pi^A + \beta_\pi^B)/2$.

S7 Semiempirical analysis

To estimate the dipole moment of a functionalized molecule, we use a set of tight-binding parameters of the host molecule and the functional group, both referred here as molecular fragments. The parameters are extracted from the Fock matrix calculated by semiempirical PM6 method [9].

Two MO sets are important for the considered system. The first one is the σ -bonding orbital by which the functional group (fragment A) is attached to the host molecule (fragment B). It is a well localized orbital. Therefore the essential parameters here are the energies, ε_σ^A and ε_σ^B , of the atomic-like orbitals (AO) constituting the bond, and the electron transfer integral, t_σ^{AB} . The self-consistent field of other electrons is important as well as the proper hybridization of the atomic s - and p -orbitals. To obtain the proper field, the hydrogen-passivated molecular fragments are used, which provide more appropriate environment than radicals or charged species. From the MO localized on the hydrogen-passivated bond we obtain the required ε_σ^A and $t_\sigma^A \equiv t_\sigma^{AH}$. Then $t_\sigma^{AB} = t_\sigma^A t_\sigma^B / t_\sigma^H$.

The second set of essential MOs is the frontier orbitals of the π -conjugated system. For this system, two important assumptions are made. First, there are no other orbitals in resonance, which is usual for π -conjugated molecules. And second, both the host molecule and the functional group are closed-shell π -systems. In this case the interaction between them can be considered perturbatively (see e.g. Ref. [8]). The relevant small parameter is the π -bond order, b_π^{AB} , of the single connecting bond arrowed in Fig. 1a (the largest calculated in this work $b_\pi^{AB} \approx 0.2$ to be compared with 1 for a single covalent bond). The second assumption excludes zwitterionic push-pull functionalization, where two functional groups, attached at the opposite sides of the conjugated molecule, are open-shell π -systems (one is a donor and another one is an acceptor). Finally, for the six functional groups considered in the following subsections, HOMO and LUMO are isolated from other MOs (among other groups, benzene has doubly degenerate HOMO/LUMO, but one of the two symmetry adapted degenerate MOs has a node on the bridging carbon). Therefore, the essential parameters of the π -system are the energies of the HOMO, $\varepsilon_{\pi0}$, and LUMO, $\varepsilon_{\pi1}$, as well as the value of each of these MOs at the bridging atom, ψ_0 for HOMO and ψ_1 for LUMO (one π -AO per atom approximation). All the tight-binding parameters introduced above are collected in Table S4.

Group	$\varepsilon_{\pi0}$	ψ_0	$\varepsilon_{\pi1}$	ψ_1	ε_σ	t_σ	t_π	$d_{ }$ (D)
NH ₂	-9.1	1	—	—	-11.9	13.4	3.8	-1.8
Me	-13.7	0.8	+6.0	0.6	-6.8	11.2	2.1	-0.7
OMe	-10.5	0.9	+5.3	0.1	-12.2	12.6	3.6	-0.5
Vi	-10.7	0.7	+1.2	0.7	-7.4	11.5	2.5	-0.0
Ph	-9.6	0.6	+0.4	0.6	-7.7	11.6	2.5	0
OH	-11.9	1	—	—	-12.9	13.1	3.5	0.4
CCH	-11.6	0.7	+1.6	0.7	-9.2	12.2	2.7	0.6
BH ₂	—	—	-0.3	1	-4.9	9.4	2.4	0.9
F	-15.8	1	—	—	-10.9	11.4	2.7	1.6
Br	-11.1	1	—	—	-9.4	8.8	1.7	1.8
COOH	-12.5	0.1	+0.2	0.8	-11.5	11.6	2.4	2.4
CHO	-14.8	0.6	+0.0	0.8	-9.5	11.4	2.4	2.6
CN	-14.1	0.7	+1.0	0.7	-11.2	12.0	2.5	4.1
NO ₂	-12.3	0	-1.0	0.7	-16.0	12.8	2.7	5.3

Table S4: Essential tight-binding parameters (in eV) and estimated $d_{||}$ for selected functional groups. The last two columns are for functional groups attached to phenyl. *Notes:* For NH₂ the planar conformation is used. The π -system of Me and OMe is mixed with other orbitals through the sp^3 -hybridized carbon.

The formulas for calculating electronic properties of A+B system based on the tight-binding parameters of the fragments A and B are derived in Section S6. In particular, the predicted by Eq. (S13) dipole moment for the test set given in Table S4 is compared with full-molecule calculations in Fig. S8. Overall, the agreement between the two sets is satisfactory: the coefficient of determination $R^2 = 0.85$ (we remind that the theory has no adjustable parameters). The major error source is the determination of the self-consistent t_π : if we take its exact value the R^2 increases to 0.91.

It should be noticed that the above approach takes into account the chemical bonding between fragments,

but neglects the mutual physical polarization (diagonal perturbation in the notations of Section S5). The latter leads, for example, to uniform downshift of MO energies of the composite system with respect to the isolated fragments. The polarization effects may be important when the chemical bonding is weak, in particular, for heavy atoms with small π -coupling such as Br. Also, the sp -hybridization is weak for heavy atoms resulting in small energy difference between the σ -bonding MO and π -HOMO (in the above approach they are considered independently).

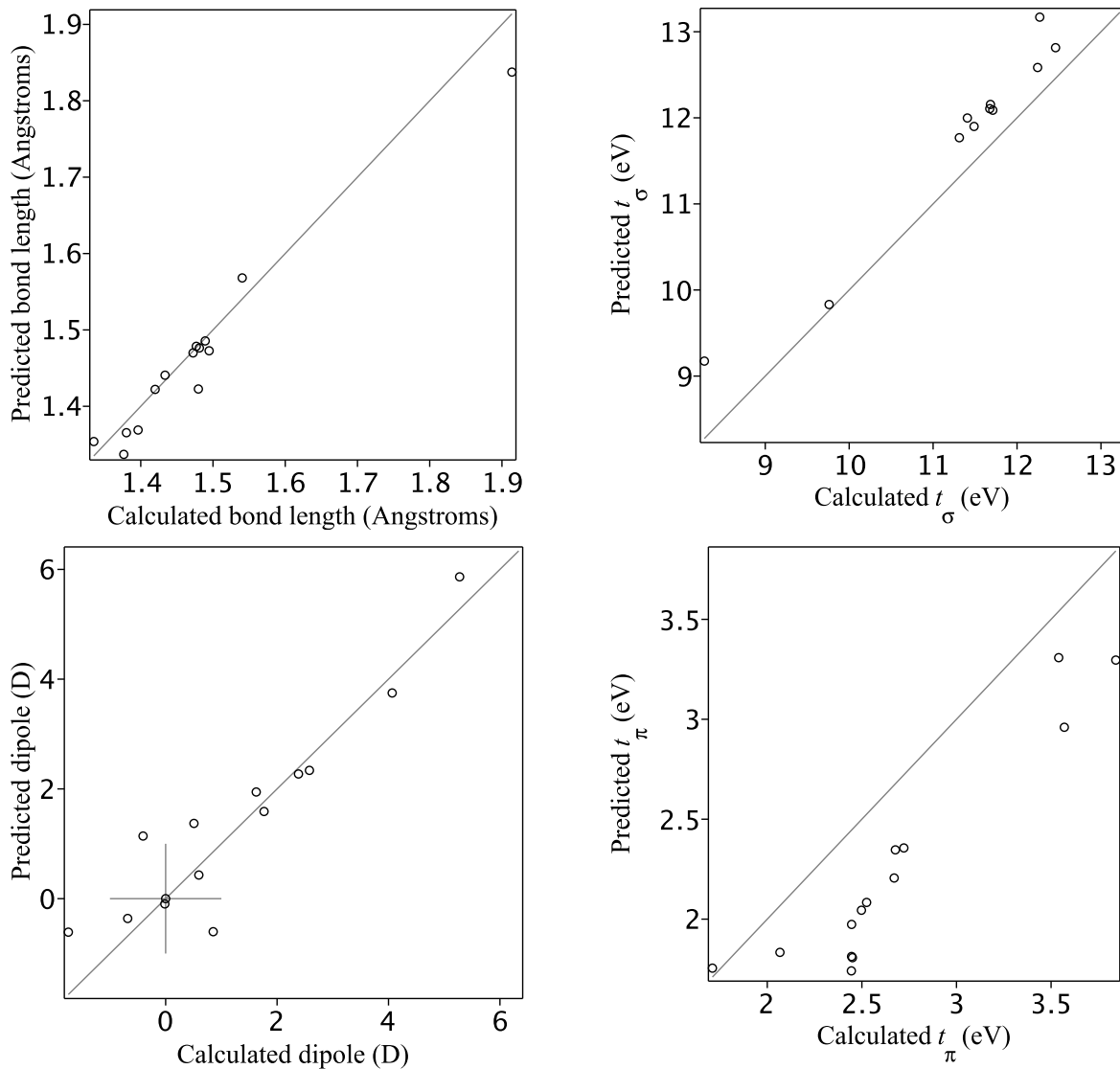


Figure S8: Calculated (PM6) vs. predicted parameters for the test set from Table S4.

S8 Localized molecular orbitals analysis

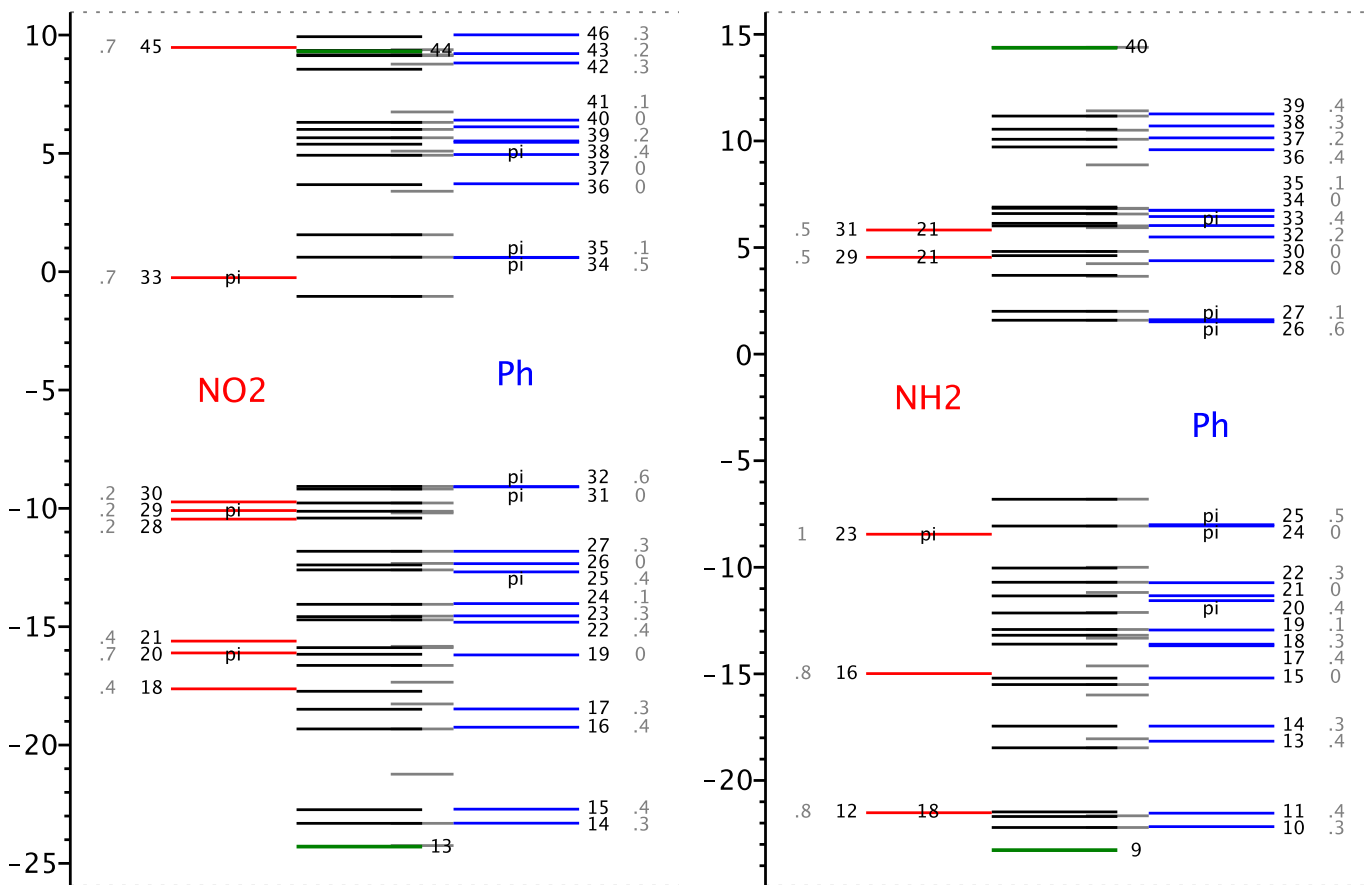


Figure S9: MO partitioning among functional group and host molecule. The black colored set of MOs at the center are the eigenvalues of the Fock matrix of the entire molecule. The two green colored levels at the center are bonding and antibonding NBOs localized on the bridging bond. The red and blue sets corresponds to the eigenvalues of the orthogonal projections of the Fock matrix onto each of the two fragments obtained using NBO basis. Red, green, and blue orbitals together form a complete basis and are numbered according to their energy. They can be visualized in Jmol program using the provided supplementary files with the filename “mo_*+ph.mgf”, where “**” must be replaced by the group chemical formula. The gray colored numbers are the values of MO wave-function on the bridging atom. Label “pi” means π -orbital, a number in place of “pi” means π -content of the corresponding orbital, no label means zero π -content. The light red and light blue sets correspond to hydrogen passivated fragments. Interfragment orbital interactions within the second order perturbation theory are listed in “mo_*+ph.txt” files. In particular, charge transfer and MO energy shift are calculated by the formulas $\Delta n = 2t^2/\Delta\varepsilon^2$ and $\Delta E_{MO} = \sqrt{t^2 + \Delta\varepsilon^2/4} - |\Delta\varepsilon|/2$ respectively, where t and $\Delta\varepsilon$ are electron transfer integral and energy difference between a pair of interacting MOs.

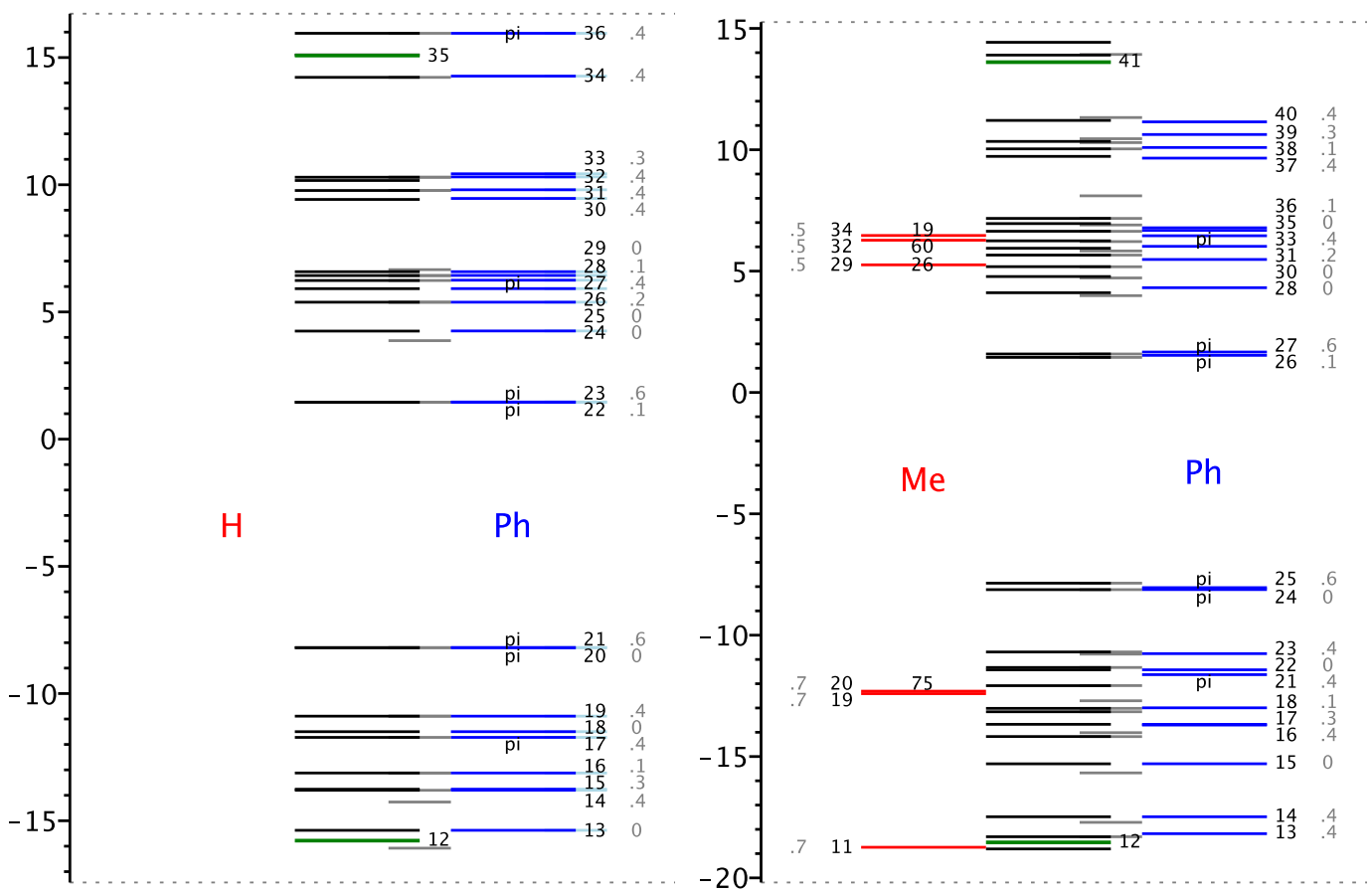


Figure S10: MO partitioning among functional group and host molecule. See Fig. S9 for details.

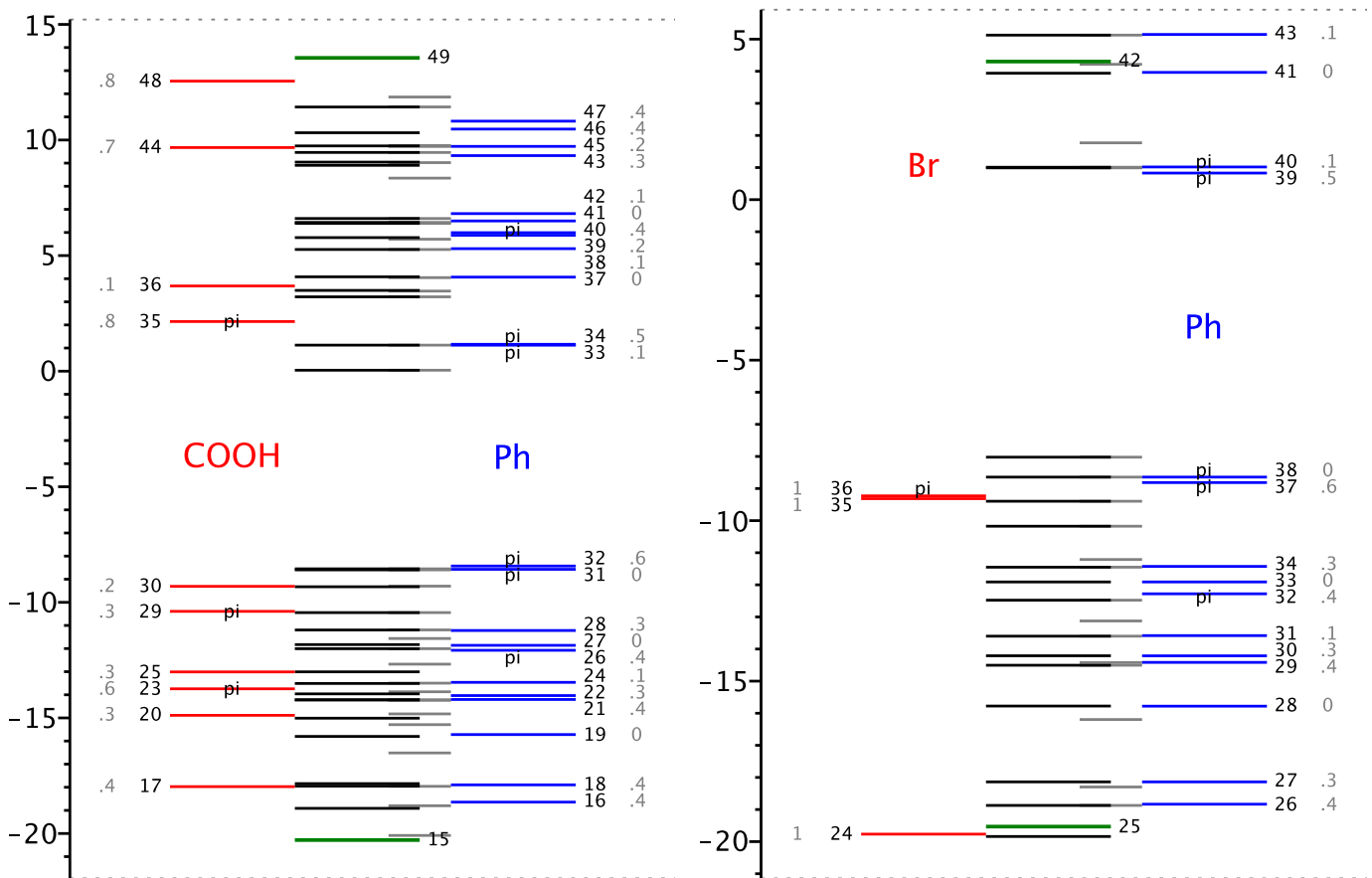


Figure S11: MO partitioning among functional group and host molecule. See Fig. S9 for details.

S9 Molecular and natural orbitals (basis set 6-31G)

Group $\delta d_{\parallel}(D)$	HOMO	LUMO
NH ₂ -1.91		
Me -0.34		
H 0		
Br +0.79		
COOH +1.23		
NO ₂ +1.83		

Table S5: Frontier molecular orbitals in vacuum.

	Hole NTO/NO/HOMO	Electron NTO/NO/LUMO
MO, GS, vacuum $n_h = 2$ $n_e = 0$		
NO, vacuum $n_{h/e} = 1$ $\Delta n_2 = 0.025/0.023$		
NO, acetonitrile $n_{h/e} = 1$ $\Delta n_2 = 0.023/0.024$		
NTO, GS, vacuum $n_{h/e} = 1 \pm 0.042$		
NTO, ES, vacuum $n_{h/e} = 1 \pm 0.029$		
NTO, GS, DMSO $n_{h/e} = 1 \pm 0.043$		
NO-ES, GS, vacuum $n_h = 1 + 0.046$ $n_e = 1 - 0.041$		

Table S6: Comparison of different molecular orbitals for H-OPV3 using CAM-B3LYP functional.

	Hole NTO/NO/HOMO	Electron NTO/NO/LUMO
MO, GS, vacuum $n_h = 2$ $n_e = 0$		
NO, CS, vacuum $n_{h/e} = 1$ $\Delta n_2 = 0.025/0.027$		
NO, CS, acetonitrile $n_{h/e} = 1$ $\Delta n_2 = 0.022/0.018$		
NTO, GS, vacuum $n_{h/e} = 1 \pm 0.047$		
NTO, ES, vacuum $n_{h/e} = 1 \pm 0.037$		
NTO, GS, DMSO $n_{h/e} = 1 \pm 0.041$		
NO-ES, GS, vacuum $n_h = 1 + 0.163$ $n_e = 1 - 0.150$		

Table S7: Comparison of different molecular orbitals for $\text{NO}_2\text{-OPV3}$ using CAM-B3LYP functional.

	Hole NTO/NO/HOMO	Electron NTO/NO/LUMO
MO, GS, vacuum $n_h = 2$ $n_e = 0$		
NO, CS, vacuum $n_{h/e} = 1$ $\Delta n_2 = 0.035/0.040$		
NO, CS, acetonitrile $n_{h/e} = 1$ $\Delta n_2 = 0.028/0.020$		
NTO, GS, vacuum $n_{h/e} = 1 \pm 0.114$		
NTO, ES, vacuum $n_{h/e} = 1 \pm 0.071$		
NTO, GS, DMSO $n_{h/e} = 1 \pm 0.097$		
NO-ES, GS, vacuum $n_h = 1 + 0.115$ $n_e = 1 - 0.114$		

Table S8: Comparison of different molecular orbitals for $\text{NO}_2\text{-OPV3}$ using ωB97X functional.

	Hole NTO/NO/HOMO	Electron NTO/NO/LUMO
MO, GS, vacuum $n_h = 2$ $n_e = 0$		
NO, CS, vacuum $n_{h/e} = 1$ $\Delta n_2 = 0.007/0.006$		
NO, CS, acetonitrile $n_{h/e} = 1$ $\Delta n_2 = 0.007/0.009$		
NTO, GS, vacuum $n_{h/e} = 1 \mp 0.001$		
NTO, ES, vacuum $n_{h/e} = 1 \mp 0.001$		
NTO, GS, DMSO $n_{h/e} = 1 \mp 0.001$		
NO-ES, GS, vacuum $n_h = 1 + 0.800$ $n_e = 1 - 0.822$ $\Delta n_2 = 0.001/0.001$		

Table S9: Comparison of different molecular orbitals for $\text{NO}_2\text{-OPV3}$ using B3LYP functional.

S10 UV-Vis absorption spectra

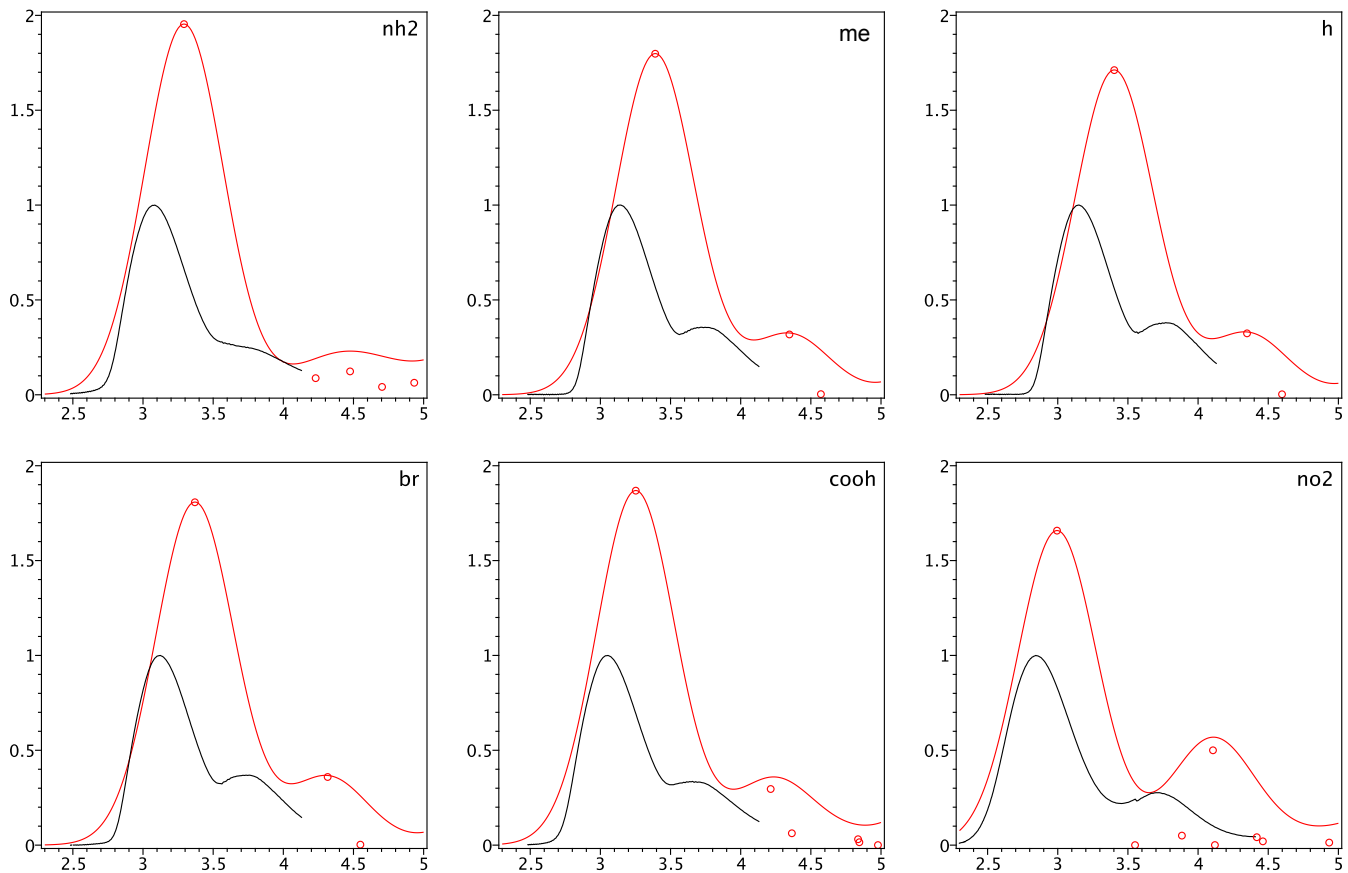


Figure S12: UV-Vis absorption spectra (shown as transition spectral density) in chloroform: experiment at the concentration 10^{-4} M (black curve, amplitude normalized to 1) versus simulation (red curve) obtained by Gaussian broadening ($\sigma = 0.28$ eV) of the individual electronic transitions shown by red dots (CAM-B3LYP/6-31G). The abscissa is in eV, the ordinate marks the oscillator strengths.

S11 NTO analysis of the second absorption band

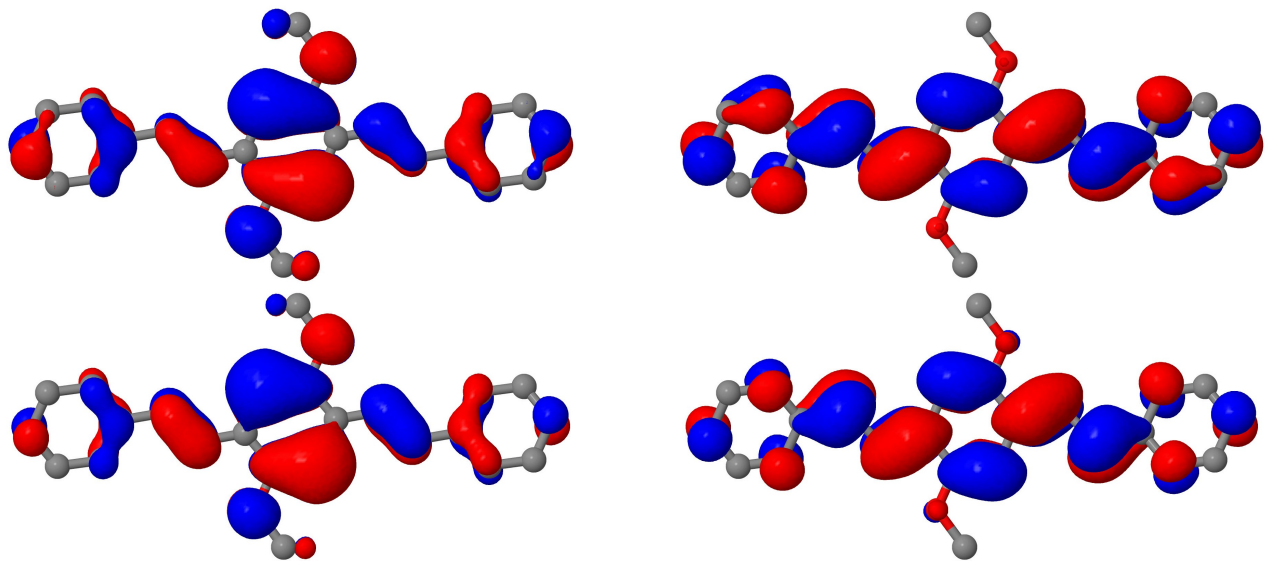


Figure S13: The electronic transition producing the second absorption band of H-OPV3. Top: HOMO-1 (left) and LUMO (right). Bottom: hole (left) and electron (right) NTO for the transition.

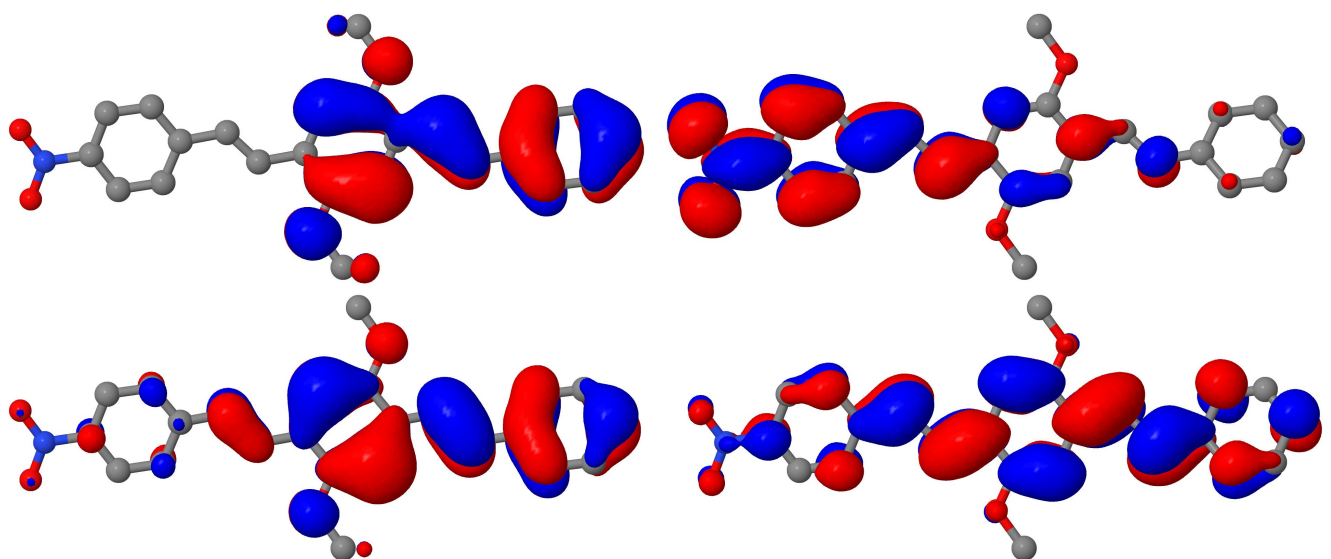


Figure S14: The electronic transition giving the main contribution corresponding to the second absorption band of NO₂-OPV3. Top: HOMO-1 (left) and LUMO (right). Bottom: hole (left) and electron (right) NTO for the transition. In this case there is no clear correspondence between NTOs and MOs, due to the dense excitation spectrum (multiple competing transitions).

S12 Vibronic couplings

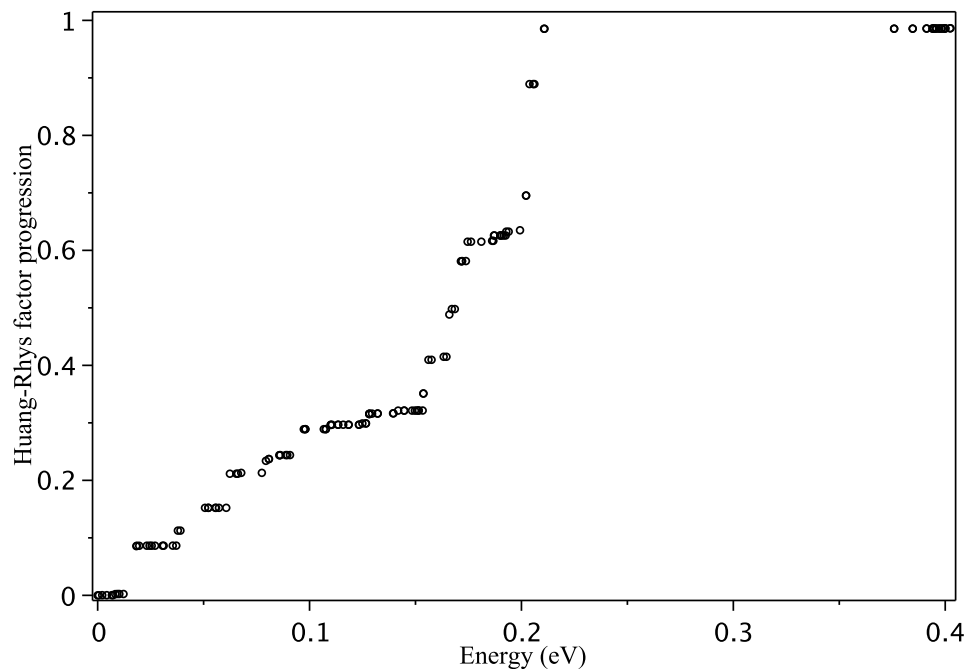


Figure S15: Huang–Rhys factor progression with the mode energy: H-OPV3 calculated by B3LYP/6-31G.

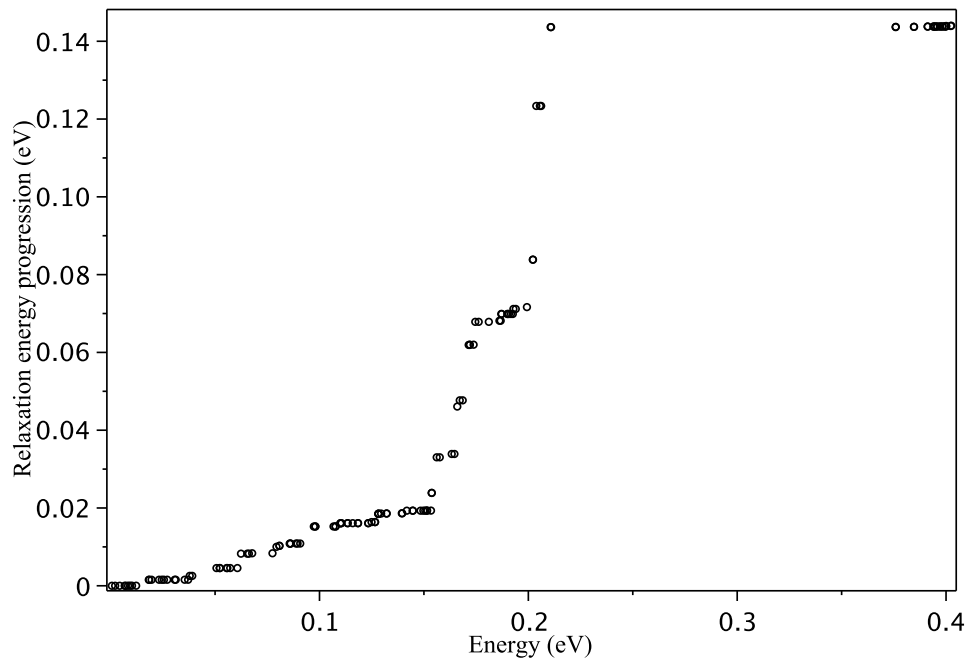


Figure S16: Exciton relaxation energy progression with the mode energy: H-OPV3 calculated by B3LYP/6-31G.

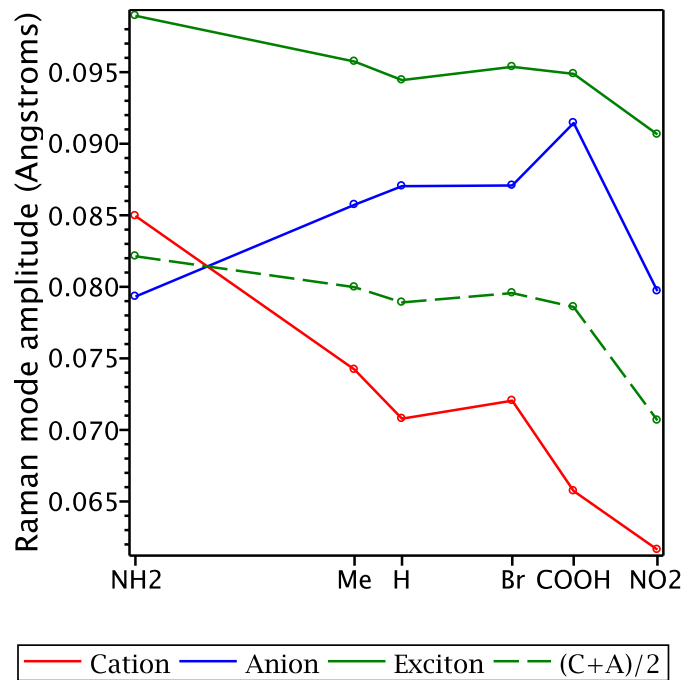


Figure S17: Amplitudes of the Raman strongest BLA-patterned mode [11] relative to the ground state geometry. It is a superposition of nearly degenerate vibrational modes at around 0.2 eV with the strongest vibronic couplings, see Figs. S15 and S16.

S13 Comparison of density functionals used in this work

Functional	ω , bohr $^{-1}$	X-HF, $c_{\text{SR}}/c_{\text{LR}}$	X-DF(α_x)	C-DF(α_c)
B3LYP	—	0.2	B88(0.9)	LYP(0.81)
CAM-B3LYP	0.33	0.19 / 0.65	B88	LYP(0.81)
ω B97X	0.3	0.16 / 1	B97'	B97

Table S10: Short description of the functionals used in the DFT calculations. The given parameters enter the total exchange-correlation energy as follows: $E_{xc} = c_{\text{SR}}E_x^{\text{HF},\text{SR}} + c_{\text{LR}}E_x^{\text{HF},\text{LR}} + (1 - c_{\text{SR}})E_x^{\text{DF},\text{SR}} + (1 - c_{\text{LR}})E_x^{\text{DF},\text{LR}} + E_c^{\text{DF}}$, where $E_{x,c}^{\text{DF}} = E_{x,c}^{\text{DF,local}} + \alpha_{x,c}\Delta E_{x,c}^{\text{DF,nonlocal}}$, omitted α implies $\alpha = 1$, X means exchange, C means correlation, HF = Hartree–Fock, DF = density functional, SR(LR) means short(long)-range, ω is the range separation parameter, other notations see in Refs. [12, 13].

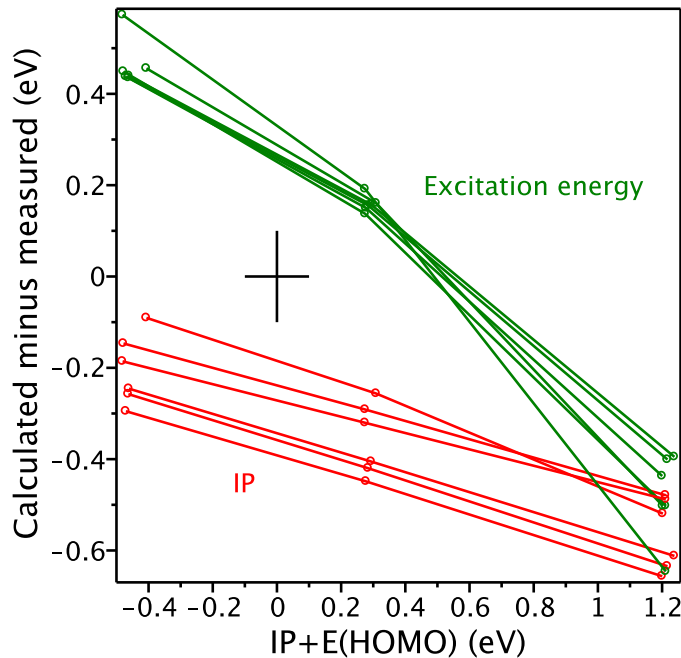


Figure S18: Correlation between $\text{IP} + E_{\text{HOMO}}$, and errors in IP (red) and excitation energy (green). The dataset covers six functional groups and three density functionals.

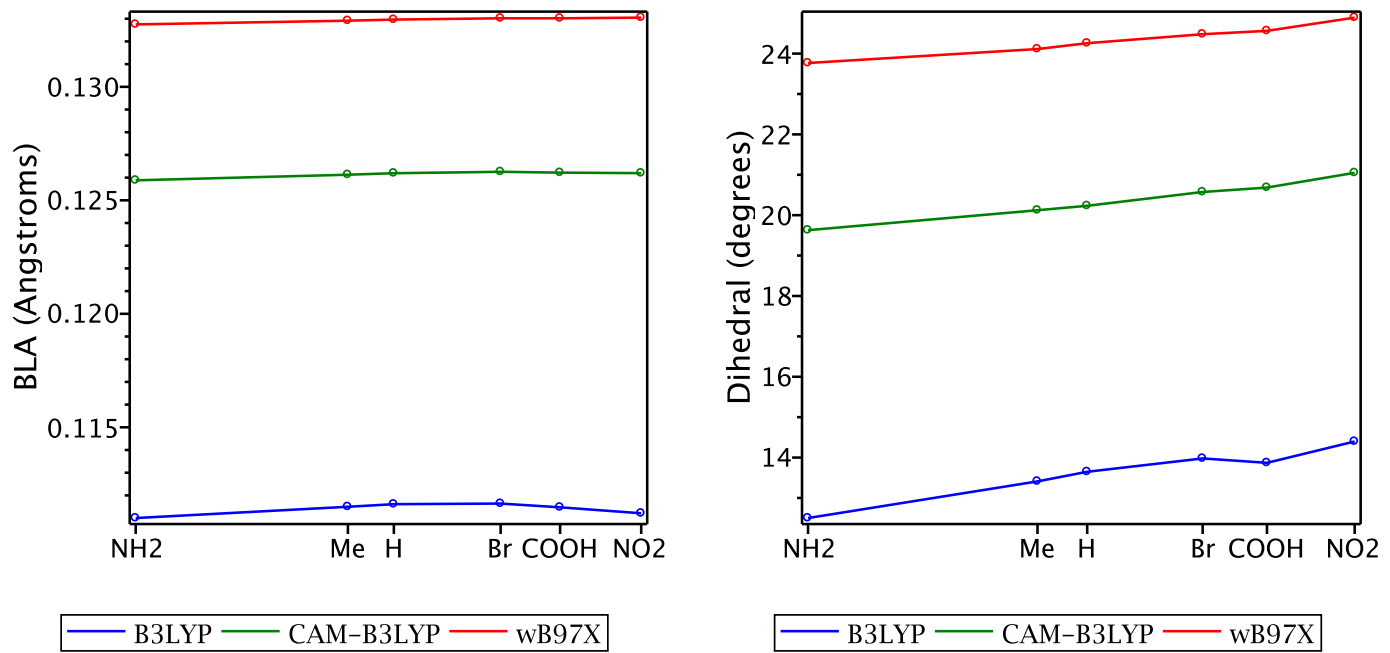


Figure S19: Dependence of BLA β_1 and dihedral δ_1 on density functional.

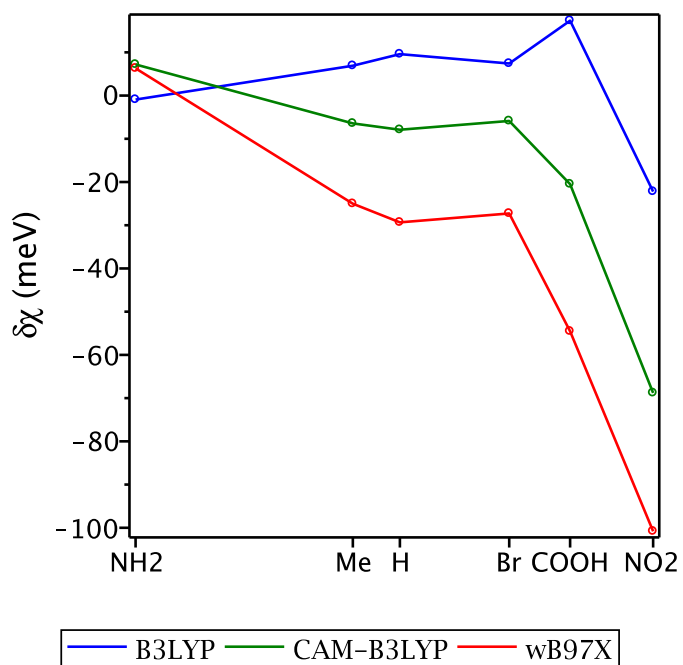


Figure S20: Dependence of $\delta\chi$ on functional group and density functional.

S14 Comparison of basis sets used in this work

Basis set	size	N_{prim}	$E(\text{meV})$
6-31G**	500	882	0
6-31G*	434	816	18
6-31G	278	660	174
cc-pVDZ	500	1012	-16
DGDZVP2	500	1060	-106
Def2SVP	500	804	454

Table S11: Comparison of different basis sets as applied to H-OPV3 molecule. Here N_{prim} is the number of primitive gaussians and E is the relative total energy per atom.

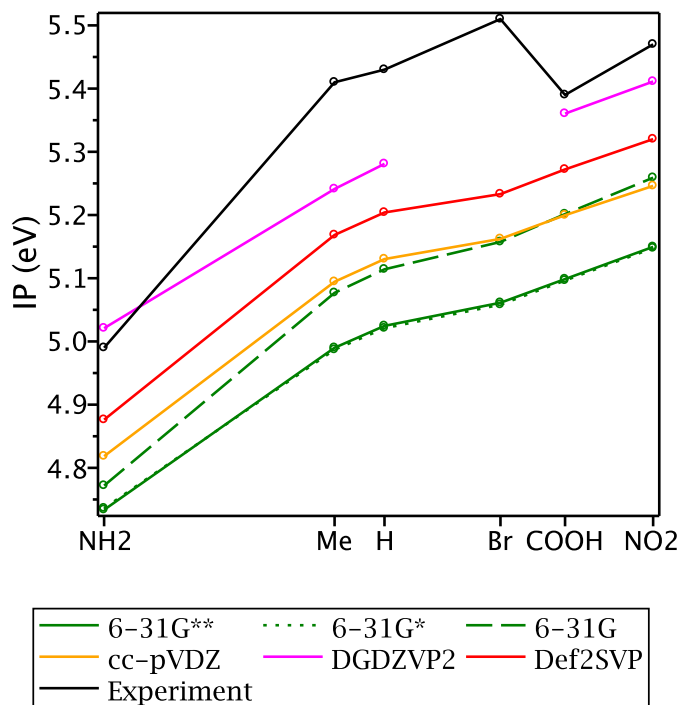
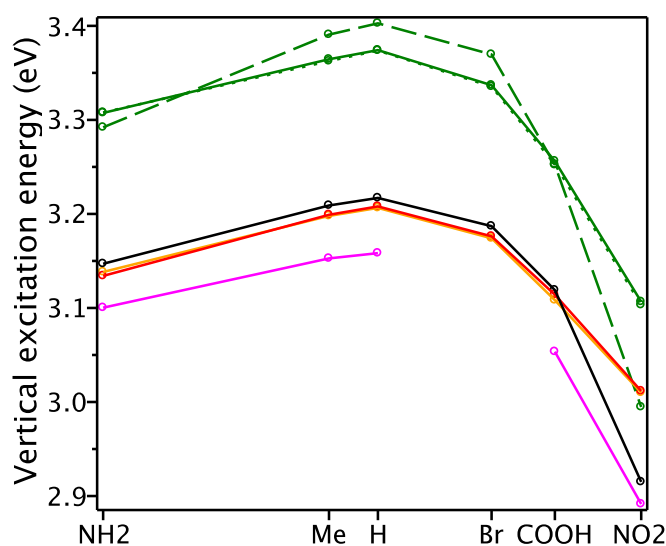
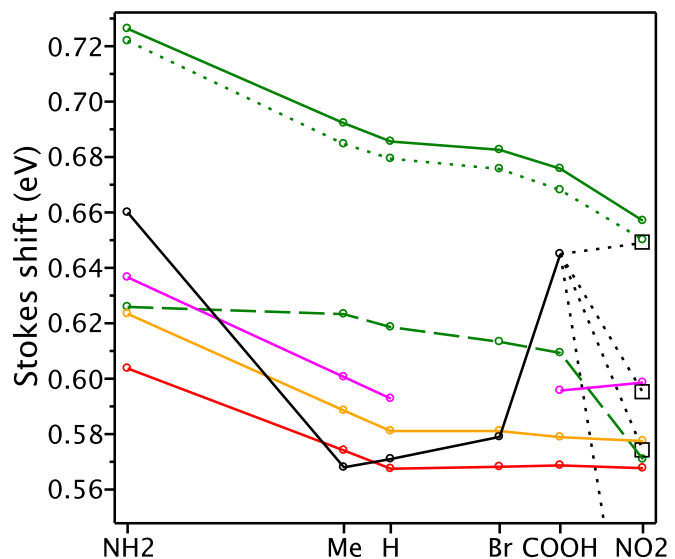


Figure S21: Experimental (cyclic voltammetry in acetonitrile) vs. predicted IP: basis set dependence.



6-31G**	6-31G*	6-31G
cc-pVDZ	DGDZVP2	Def2SVP
— Experiment		



6-31G**	6-31G*	6-31G
cc-pVDZ	DGDZVP2	Def2SVP
— Experiment		

Figure S22: Experimental (in chloroform) vs. predicted first excitaition energy and Stokes shift (LR approach): basis set dependence.

S15 Other figures and tables

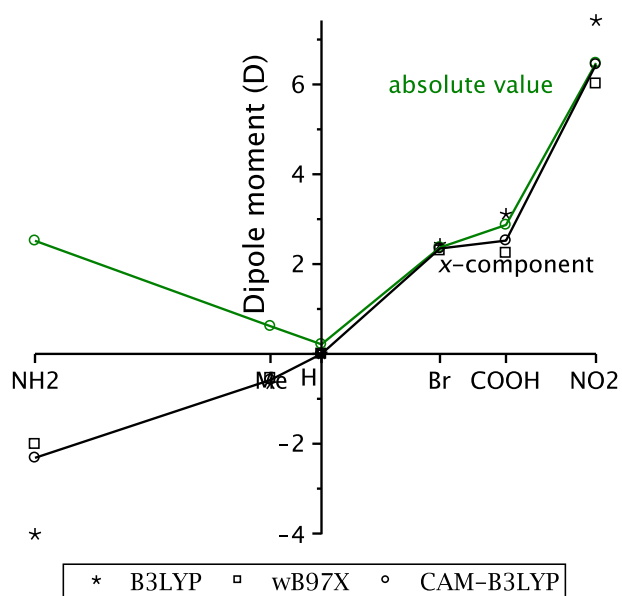


Figure S23: Dipole moments (in vacuum).

R	IP(vac)	EA(vac)	IP(acn)	EA(acn)
NH ₂	6.17	-0.01	5.05	1.64
Me	6.38	0.12	5.20	1.71
H	6.45	0.15	5.23	1.73
Br	6.54	0.32	5.27	1.80
COOH	6.59	0.49	5.30	1.98
NO ₂	6.75	0.87	5.35	2.55

Table S12: IP/EA (in eV) in vacuum and acetonitrile of R-OPV3 molecules studied in this work. Among the functional groups used for the derivation of the molecular descriptor, the less electronegative is S-OPV3 anion whose EA is -1.8 eV in vacuum and 1.6 eV in acetonitrile.

References

- [1] C Hansch, A Leo, R W Taft, A Survey of Hammett Substituent Constants and Resonance and Field Parameters, *Chem Rev* 97, 165 (1991)
- [2] NIST Chemistry WebBook, <http://webbook.nist.gov/chemistry>
- [3] T M Ramond, G E Davico, R L Schwartz, W C Lineberger, Vibronic structure of alkoxy radicals via photoelectron spectroscopy, *J Chem Phys* 112, 1158 (2000)
- [4] I Cernusak, A Zavazanova, J Raab, P Neogrady, Group IIIa hydrides XH₂ and XH₂- (X = B, Al, Ga): electron affinities and singlet-triplet splittings revisited, *Collect Czech Chem Commun* 68, 75 (2003)
- [5] Y I Park, C Kuo, J S Martinez, Y Park, O Postupna, A Zhugayevych, S Kim, J Park, S Tretiak, H Wang, Tailored electronic structure and optical properties of conjugated systems through aggregates and dipole-dipole interactions, *ACS Appl Mater Interfaces* 5, 4685 (2013)
- [6] F Jensen, *Introduction to computational chemistry* (Wiley, 2007)
- [7] J N Murrell, S F A Kettle, J M Tedder, *The chemical bond* (Wiley, 1985)
- [8] A Zhugayevych, V Lubchenko, Electronic structure and the glass transition in pnictide and chalcogenide semiconductor alloys. I. The formation of the pp σ -network, *J Chem Phys* 133, 234503 (2010)
- [9] J J P Stewart, Optimization of parameters for semiempirical methods V: modification of NDDO approximations and application to 70 elements, *J Mol Model* 13, 1173 (2007)
- [10] M J S Dewar, W Thiel, Ground states of molecules, 38. The MNDO method. Approximations and parameters, *J Am Chem Soc* 99, 4899 (1977)
- [11] G Zerbi, *Vibrational Spectroscopy of Conducting Polymers: Theory and Perspective*, in *Handbook of Vibrational Spectroscopy* (Wiley, 2006)
- [12] C J Cramer, *Essentials of computational chemistry: theories and models* (Wiley, 2004)
- [13] R Baer, E Livshits, U Salzner, Tuned range-separated hybrids in density functional theory, *Annu Rev Phys Chem* 61, 85 (2010)